affected individuals, using reverse transcription polymerase chain reaction (RT-PCR). Given the high frequency of this mutation among LQTS patients, elucidating the detailed molecular mechanisms by which this mutation affects the phenotypes of LQTS is of critical importance.

Pre-mRNA processing is an important aspect of gene expression and consists of the precise recognition of exons and removal of introns in such a way that the exons are joined to form mature mRNAs with intact translational reading frames [10,11]. Disruption of normal splicing as a result of genetic mutation can lead to the generation of abnormal proteins or the degradation of aberrant transcripts through nonsense-mediated decay, and thus to the pathogenesis of a variety of human diseases [12].

The present study was therefore designed to understand the molecular basis of the pathogenesis of LQTS caused by this relatively common splicing mutation in the KCNQ1 gene. We carried out quantitative analysis of exon-skipping transcripts of the KCNQ1 gene using real-time RT-PCR and examined how those quantitative changes may contribute to the pathogenesis using a variety of biochemical and biophysical approaches: voltage-clamp current recordings, confocal microscopy, and fluorescence resonance energy transfer (FRET) analysis.

2. Materials and methods

2.1. Genomic DNA isolation and mutation analysis

Mutation analysis was carried out as previously described [13] with our minor modifications. Genomic DNA was prepared from peripheral blood leukocytes using QIAamp DNA Blood Midi Kits (Qiagen: Valencia, CA). 16 exons of the KCNQ1 gene were amplified by PCR using intronic primer sequences. Genetic screening was performed for KCNQ1 by denaturing high-performance liquid chromatography (DHPLC) using a WAVE System Model 3500 (Transgenomic: Omaha, NE). Abnormal conformers were amplified by PCR and sequencing was performed on an ABI PRISM3100 DNA sequencer (Applied Biosystems: Foster City, CA). We also carried out a complete screening for other LQTS-causing genes; KCNH2, SCN5A, KCNE1, and KCNJ2.

2.2. RNA extraction and real-time RT-PCR

Total RNA was extracted from leukocytes of fresh blood using QIAamp RNA Blood Mini Kits (Qiagen). Subsequently, DNase-treated total RNA was reverse-transcribed by use of the SuperScriptIII FirstStrand Synthesis System (Invitrogen: Carlsbad, CA) and was used as a template for subsequent PCR reactions. We used the exon 5-F forward primer (5′-GGGCATC-CGCTTCCTGCAGA-3′) and the exon 10-R reverse primer (5′-CCATTGTCTTTGTCCAGCTTGAAC-3′) to amplify KCNQ1 cDNA from exons 5 through 10.

Measurements of normal and mutant mRNA levels were performed by real-time RT-PCR by use of an ABI PRISM 7900HT Sequence Detection System (Applied Biosystems). The reaction mixture contained SYBR Green PCR Master Mix (Applied Biosystems), cDNA template, and PCR primers. In order to selectively amplify these splicing variants, PCR primers were designed so that they spanned the adjacent exons: Exon 6.8-F: 5′-CTGTGGTGGGGGGTG-GGGATT-3′, Exon 6.9-F: 5′-TGTGGTGGGGGGTG-ACCGCAT-3′, Exon 7.9-F: 5′-CTTT-GCGCTCCCAGCG-ACCG-3′ (all the hyphens inside the primer sequence indicate the boundaries of exons). In all cases, the dissociation curves showed that there was no significant contribution of relatively short by-products to the measured fluorescence intensities.

All the samples were tested in duplicate. A standard curve for each primer pair was obtained using serial dilutions of a recombinant plasmid containing cDNA. The threshold cycle (Ct) was subsequently determined. Relative mRNA levels of splice mutants were calculated based on the Ct values and normalized by the GAPDH level of each sample. The amounts of mutant cDNA were expressed as a percentage of the total KCNQ1 mRNA, for which exons 9 through 10 were amplified with the exon 9-F forward primer (5′-CGCATGGAGGTGC-TATGCT-3′) and the exon 10-R reverse primer.

2.3. Oocyte isolation and electrophysiology

Xenopus laevis oocytes were prepared and current recordings were carried out as described previously [14]. Each KCNQ1 cRNA (10 ng) alone or wild-type (WT) cRNA (10 ng) plus mutant-cRNA (10 ng) was injected into *Xenopus* oocytes. All the current recordings in the present study were performed in the presence of KCNE1 β-subunits (1 ng). Background I_{Ks} current was recorded in oocytes injected with KCNE1 alone.

An axoclamp-2B amplifier (Axon Instruments, Union City, CA) was used to record currents at 25 °C in oocytes 4–5 days after cRNA injection, using standard two-electrode voltage-clamp techniques. To decrease the interference from endogenous Cl^- current, we used a low-Cl^- bath solution (mM): NaOH 96, KOH 2, $CaCl_2$ 2, $MgCl_2$ 1, MeS 101, HEPES 5 (pH titrated to 7.6 with methanesulfonic acid). Currents were sampled at 10 kHz and filtered at 2 kHz. Voltage steps were applied with 3-s pulses in 10 mV increments from a holding potential of −80 mV to voltages from −70 to +60 mV, and then to −30 mV, where tail currents were recorded. Current amplitudes were measured at 1.5-s after the initiation of 3-s pulse applied to a +50 mV test potential, followed by the subtraction of background I_{Ks} current (49.5 nA).

2.4. Cell preparation and confocal imaging

For confocal microscopy experiments, green fluorescent protein (GFP)-tagged KCNQ1 was constructed using EGFP-N1 vector (Clontech: Mountain View, CA). COS7 cells were plated on 35-mm glass-bottom culture dishes and maintained for 12–24 h in Dulbecco's modified Eagle's medium containing 20% FBS. Lipofection was performed with Lipofectamine reagent (Invitrogen). 48 h after transfection, COS7 cells were incubated for 24 h with 100 μM cycloheximide. The localization of GFP-tagged proteins was detected using a Zeiss laser-scanning confocal microscope (Zeiss LSM510 META) with a 63×1.40

Please cite this article as: Tsuji K, et al, Mechanistic basis for the pathogenesis of long QT syndrome associated with a common splicing mutation in KCNQ1 gene, J Mol Cell Cardiol (2007), doi:10.1016/j.yjmcc.2006.12.015

numerical aperture oil-immersion objective. GFP was excited using a 488-nm line of an argon laser and signals were collected through a 500–530 band-pass filter.

2.5. FRET

FRET imaging has been proven to be a powerful tool for detecting protein–protein interactions in living cells [15]. We used a FRET experiment protocol with acceptor photobleaching and spectral unmixing [16] with minor modifications. We constructed cyan or yellow fluorescent protein (CFP, YFP)-tagged KCNQ1 using ECFP-C1 or EYFP-C1 vector (Clontech), respectively. FRET was measured by acceptor photobleaching, where an increase in CFP signal (dequenching) during incremental photobleaching of YFP can be observed. Samples were excited with a 458-nm line of an argon laser, and confocal images were obtained before and after acceptor photobleaching (a 514-nm line of an argon laser was used to photobleach YFP), by using a 458- to 514-nm dichroic beamsplitter, and the META detector was set between 473 and 558 nm. The two temporally averaged 3D image sets (x, y and spectrum) were linearly unmixed, resulting in four 2D fluorescence data sets (the donor/acceptor before/after photobleaching). Finally, subtracting the unmixed donor emission before the photobleaching from that after photobleaching resulted in the net FRET distribution. FRET efficiency (E) was calculated as:

$$E = \frac{I_D - I_{DA}}{I_{DA}}(\%),$$

where I_{DA} is the CFP-normalized fluorescence intensity before and I_D is the CFP-normalized fluorescence intensity after photobleaching of the acceptor (YFP).

2.6. Statistical analysis

Quantitative data are presented as the mean±SEM. Multiple comparisons among groups were carried out by one-way ANOVA with Bonferroni's least significant difference as the post hoc test. A level of $p<0.05$ was accepted as statistically significant.

3. Results

3.1. Mutation analysis

Pedigrees and the clinical features for the 3 LQTS families (Family K176, K214 and K155) examined in this study are shown in Supplementary Figure. The 3 families were unrelated. DNA samples from 8 members of the families (II-6, III-2, III-3, IV-1, IV-2 in Family K176, III-1 in Family K214, and I-1, II-1 in Family K155) were subjected to a mutation screening of the KCNQ1 gene. An abnormal migration pattern was identified by DHPLC analysis (Fig. 1, left panel: note the comparable height of the left and right peaks) in KCNQ1 exon 7 of the 6 affected individuals (II-6, III-2, III-3 in Family K176, III-1 in Family K214, and I-1, II-1 in Family K155). The remaining 2 individuals

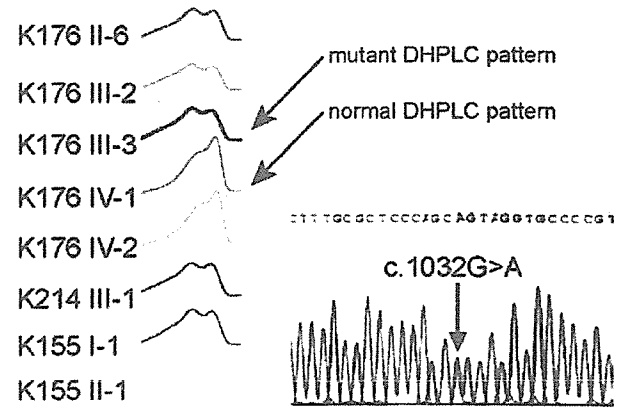

Fig. 1. Mutation analysis. Left panel: DHPLC revealed abnormal migration patterns in the affected individuals. Right panel: Automated DNA sequencing electropherogram demonstrates c.1032G>A mutation.

(IV-1, IV-2 in K176) showed normal patterns, as indicated by the greater height of the right peak (Fig. 1, left panel). DNA sequencing identified a heterozygous guanine to adenine change in KCNQ1 at nucleotide 1032 (c.1032G>A) (Fig. 1, right panel), which is the last base of exon 7. Among our entire group of KCNQ1-related LQTS patients, the frequency of this mutation was remarkably high (we found this mutation in 3 out of 22 families with KCNQ1 mutations, among a total of 185 families with LQTS). We ruled out the presence of mutations in other LQTS-causing genes (KCNH2, SCN5A, KCNE1, and KCNJ2).

3.2. Identification of exon-skipping KCNQ1 mRNAs using RT-PCR

To directly show the presence of exon-skipping transcripts, a total RNA sample from the proband of Family K176 was subjected to RT-PCR (Fig. 2a), using primers spanning exons 5 through 10. RNA samples were available only from the family. In contrast with the single WT band identified in normal individuals, the affected individual had shorter bands as well as the normal-sized WT. The direct sequencing of these short-sized transcripts revealed the existence of three kinds of exon-skipping mRNAs (Δ7–8:399 bp, Δ7: 495 bp, Δ8: 510 bp, WT: 606 bp). The previous report identified Δ8 and Δ7–8 mRNAs (referred as Δ7 and Δ6–7 in this report) [7], but we additionally identified Δ7 mRNA in this study. Fig. 2b shows a schematic structure of KCNQ1 channel subunit. Similar to other voltage-gated K^+ channel α-subunits, the KCNQ1 protein has six transmembrane domains (S1–S6), a voltage sensor (S4) and a pore helix selectivity filter segment (P-loop) that connects S5 and S6. Exon 7 spans from part of the P-loop to part of the S6 region. Exon 8 constitutes the rest of S6 and part of the intracellular C-terminal domain.

3.3. Quantification of exon-skipping KCNQ1 mRNAs using real-time RT-PCR

We carried out quantitative analysis of short-sized mutant mRNAs in 3 affected members of Family K176, using real-time

Please cite this article as: Tsuji K, et al. Mechanistic basis for the pathogenesis of long QT syndrome associated with a common splicing mutation in KCNQ1 gene. J Mol Cell Cardiol (2007), doi:10.1016/j.yjmcc.2006.12.015

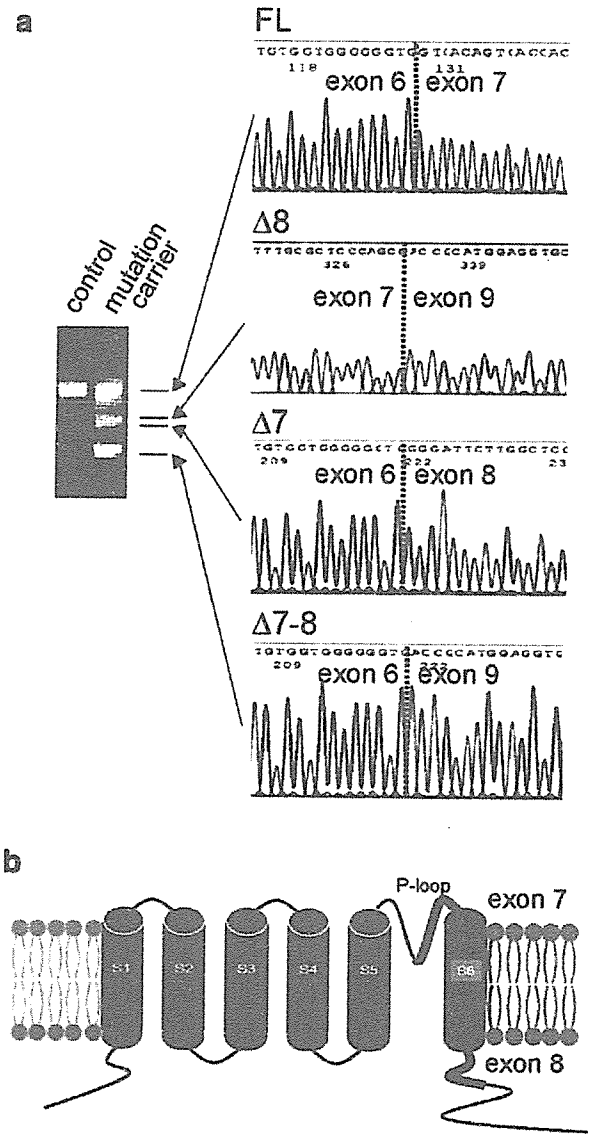

Fig. 2. Identification of exon-skipping mRNAs using RT-PCR. (a) RT-PCR from lymphocytes of a control and a mutation carrier. Nucleotide sequence of each of the exon-skipping mRNAs is also shown. (b) Scheme of the transmembrane topology of the cardiac KCNQ1 channel illustrating the location of the mutation (red asterisk) and that of exons 7 (green) and 8 (blue). The cardiac KCNQ1 channel α-subunit consists of 6 transmembrane-spanning segments (S1 through S6), and S5 and S6 are connected by the P-loop.

RT-PCR. In order to selectively amplify these splicing variants, PCR primers were designed so that they spanned the adjoining exons (Fig. 3a). Fig. 3b shows a representative amplification plot of Δ7–8 for controls ($n=4$), mutation carriers ($n=3$) and no template control, indicating the increases of the Δ7–8 mRNA in mutation carriers. Compared with normal individuals who had minor fractions of splicing variants (WT: 93.0±0.7%, Δ7: 0.0±0.0%, Δ7 8: 0.1±0.0%, Δ8: 6.9±0.7%, of total KCNQ1 transcripts; $n=4$), the affected individuals showed significant increases of exon-skipping mRNAs (WT: 55.2±0.9%, Δ7: 23.5±1.7%, Δ7 8: 16.8±0.9%, Δ8: 4.5±0.7%; $n=3$) (Fig. 3c).

3.4. Biophysical characteristics of exon-skipping KCNQ1 proteins

Electrophysiological properties of mutant KCNQ1 proteins were characterized in *X. laevis* oocytes injected with cRNA of WT or mutants (Δ7, Δ7–8, Δ8) (Fig. 4). In the *Xenopus* oocytes injected with WT, depolarizing pulses evoked time-

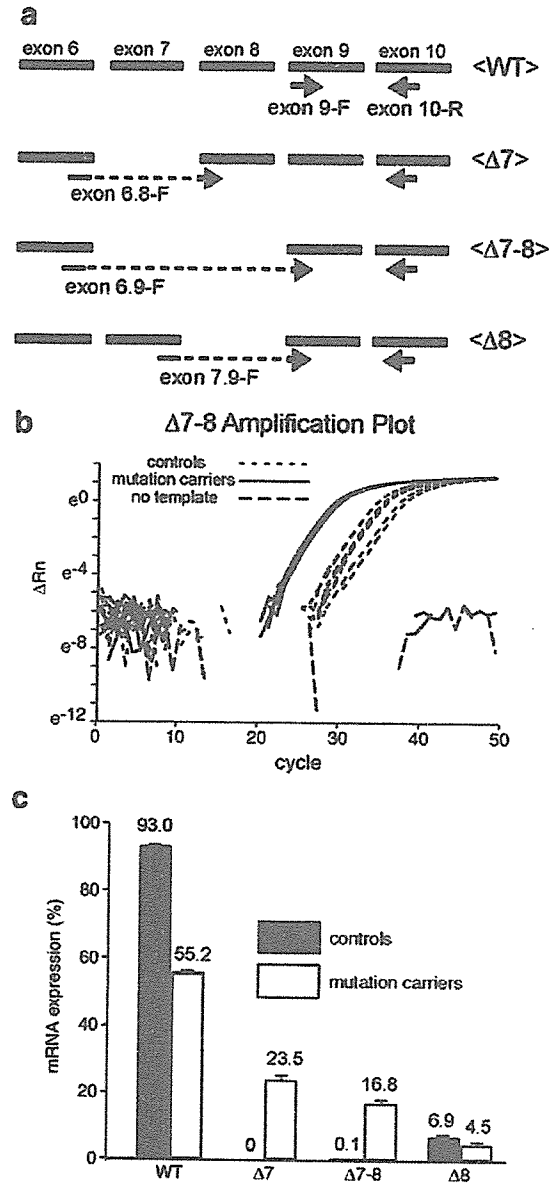

Fig. 3. Real-time RT-PCR analysis. (a) Scheme of the real-time PCR primers used to quantify the splicing mutants. A common reverse primer, exon 10-R located in exon 10, was used. Specific amplification of each splice mutant was performed with specific forward primers spanning the adjacent exons: exon 6.8-F primer for Δ7 mRNA, exon 6.9-F primer for Δ7–8 mRNA, and exon 7.9-F primer for Δ8 mRNA. (b) Representative amplification plot of Δ7–8 in real-time PCR analysis, indicating the increases of the Δ7–8 mRNA in mutation carriers. (c) Percentages of WT and mutant mRNAs. The amounts of mutant mRNA were expressed as a percentage of the total KCNQ1 mRNA. Data are the mean ± SEM. Controls: 4 normal healthy individuals. Mutation carriers: 3 members of Family K176.

Please cite this article as: Tsuji K, et al. Mechanistic basis for the pathogenesis of long QT syndrome associated with a common splicing mutation in KCNQ1 gene. J Mol Cell Cardiol (2007), doi:10.1016/j.yjmcc.2006.12.015

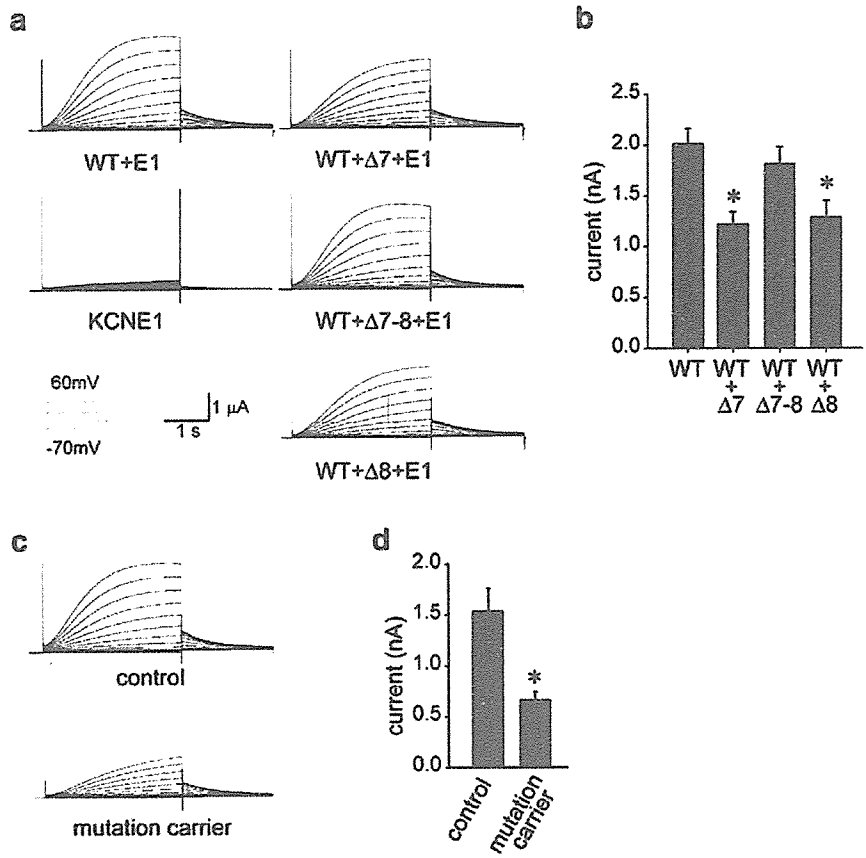

Fig. 4. Electrophysiological analysis. (a) Representative current traces recorded from two-electrode voltage-clamp of *X. laevis* oocytes heterologously expressing channels of WT or exon-skipping KCNQ1. Currents were recorded at various membrane potentials from −70 to +60 mV for 3 s in 10 mV increments from a holding potential of −80 mV. WT: 10 ng of WT cRNA was injected. WT + mutant (either Δ7, Δ7–8 or Δ8): 10 ng of WT plus 10 ng of mutant cRNA. All the current recordings in the present study were performed in the presence of KCNE1 β-subunits (1 ng). Background I_{Ks} current was recorded in oocytes injected with KCNE1 alone. (b) Pooled data of currents. Current amplitudes were measured at 1.5 s after the initiation of 3-s pulse applied to a +50 mV test potential. Background I_{Ks} current (49.5 nA) was subtracted. $n=8$ for WT, 8 for WT + Δ7, 8 for WT + Δ7–8, and 11 for WT + Δ8. $^*p<0.01$ vs. WT. (c) Representative current traces recorded from oocytes simulating the proportions of mRNA of control individuals and mutation carriers. A total of 10 ng of cRNA was injected with the relative ratios of WT and mutant KCNQ1 inferred from the data obtained in the real-time RT-PCR experiment. (d) Pooled data of currents. $n=6$ for control, and 6 for mutation carriers. $^*p<0.01$ vs. control.

dependent outward currents, indicating typical I_{Ks} channel properties (Fig. 4a, upper left panel). Background I_{Ks} current obtained in oocytes injected with KCNE1 alone was small (49.5 nA) (Fig. 4a, lower left panel). The *Xenopus* oocytes injected with Δ7, Δ7–8, or Δ8 alone displayed no time-dependent currents (data not shown), indicating that these mutants are non-functional.

To assess the functional interaction between WT and mutant channels, we co-expressed WT cRNA (10 ng) plus either one of the mutant cRNA (10 ng). The activated current amplitude of WT was 2.01±0.15 μA ($n=11$) (Figs. 4a, b). The current amplitudes with WT plus mutant KCNQ1 were recorded, and some of them were significantly smaller than those of WT (WT + Δ7: 1.22±0.12 μA, $n=8$, $p<0.01$; WT + Δ7–8: 1.82±0.16 μA, $n=8$, $p=0.34$; WT + Δ8: 1.29±0.16 μA, $n=11$, $p<0.01$) (Figs. 4a, b). These data clearly show that each exon-skipping KCNQ1 protein had the mutant-specific level of dominant-negative effect on WT channels.

In order to simulate the electrophysiological properties of cardiac cells of the affected patients, we injected the cRNAs (total 10 ng) with the relative ratios of WT and mutant KCNQ1 inferred from the data obtained in the real-time RT-PCR experiment. Cells with the cRNA ratios of the patients showed pronounced reduction in currents compared with those with the ratios of normal individuals: 1.55±0.22 μA ($n=6$) for control, 0.67±0.08 μA ($n=6$) for mutation carriers ($p<0.01$) (Figs. 4c, d). This profound suppression of I_{Ks} current may underlie the pathophysiology of these patients.

3.5. Subcellular localization of exon-skipping KCNQ1 proteins

To further explore the molecular basis of the dominant-negative effects of exon-skipping KCNQ1 proteins, we examined the subcellular localization using GFP-tagged KCNQ1 heterologously expressed in COS7 cells (Fig. 5). WT-GFP (Fig. 5a) appeared to be expressed on the plasma membrane

Please cite this article as: Tsuji K, et al, Mechanistic basis for the pathogenesis of long QT syndrome associated with a common splicing mutation in KCNQ1 gene. J Mol Cell Cardiol (2007), doi:10.1016/j.yjmcc.2006.12.015

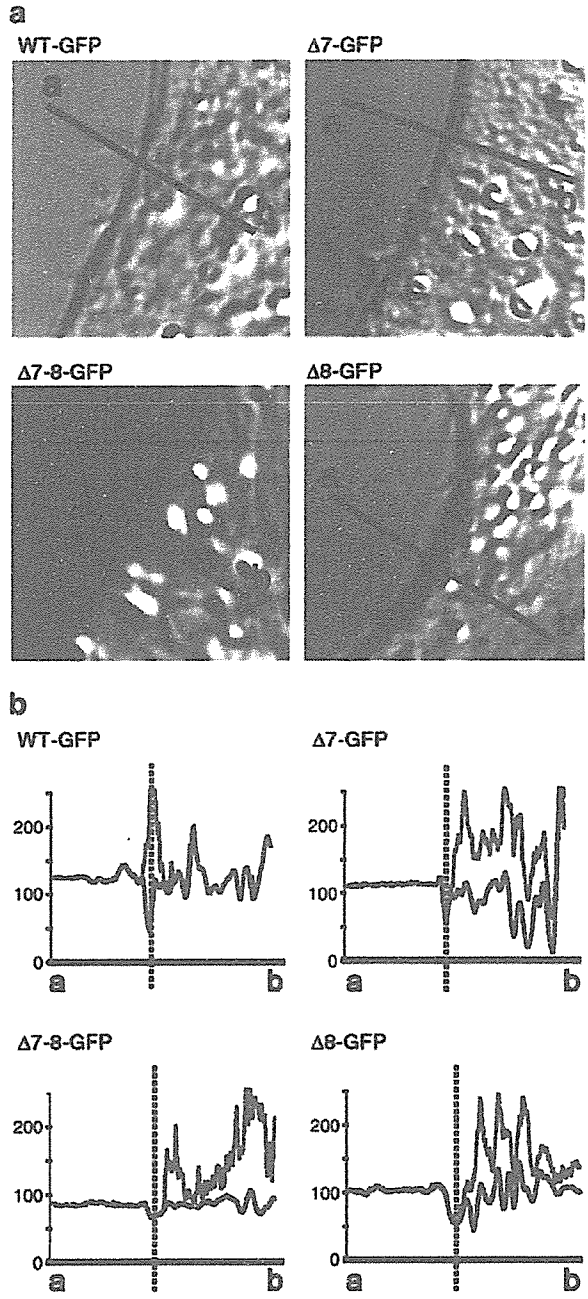

Fig. 5. Confocal microscopy analysis. (a) Overlay of transmitted bright-field image (gray) and GFP fluorescence image (green). (b) Line profile of pixel intensities (black: bright field; green: GFP) from the a-b line drawn in panel a. Vertical dashed lines represent the position of the plasma membrane. These results were representative ones obtained from at least three independent experiments.

(upper left); overlay with bright-field image (gray scale) showed green fluorescence along the plasma membrane. In the line profiles (Fig. 5b), the first major deflection in the black lines (bright-field) was defined as the plasma membrane (as indicated by the dashed vertical lines). WT-GFP had a peak at the level of the plasma membrane. In contrast, all of the mutants were retained in the cytoplasmic compartment, and GFP peaks appeared inside the cell, but not on the level of the plasma membrane (Fig. 5). These data clearly indicate that mutant KCNQ1 proteins were unable to translocate to the plasma membrane.

3.6. Direct interaction between WT and exon-skipping KCNQ1 proteins

The dominant-negative effects of the mutants suggest that they may suppress the trafficking of the WT channel to the plasma membrane. We examined this possibility by employing the co-expression of WT-YFP and Δ7-CFP (Fig. 6a). WT, which was predominantly expressed on the plasma membrane when expressed alone (data not shown, but see Fig. 5a), was retained in the intracellular compartment with remarkably reduced plasma membrane expression in the presence of Δ7. Furthermore, WT-YFP co-localized with Δ7-CFP, as shown in the merged image (Fig. 6a, upper three panels).

We then performed the FRET experiment with the acceptor bleaching method to detect the direct interaction between WT and mutant KCNQ1 subunits. The increase in CFP fluorescence intensity after YFP bleaching (Fig. 6a, lower panels) indicates that Δ7 physically interacted with the WT subunit in an intracellular compartment and prevented it from translocating into the plasma membrane.

Fig. 6b shows the summarized data regarding FRET efficiency. As for negative controls, we employed WT-CFP alone (second-to-the-right bar) and CFP plus YFP (the right-most bar). The FRET efficiency between WT and all the mutants was significantly larger than that of the negative controls ($^{*}p<0.05$ vs. WT-CFP, $^{\#}p<0.05$ vs. CFP plus YFP). Hence, all of the mutants showed the mutant-specific degree of direct interaction with the WT subunit.

4. Discussion

We performed biochemistry, electrophysiology, and cellular imaging studies to examine the behavior of WT and mutant channel subunits created by the relatively common KCNQ1 splicing mutation and provided deeper mechanistic insights into the pathogenesis of LQTS caused by this mutation.

4.1. Generation of exon-skipping KCNQ1 mRNAs

In eukaryotic cells, removal of introns from pre-mRNAs by pre-mRNA splicing is an essential process for gene expression [10,17]. Splicing is a tightly-regulated part of RNA processing, and its abnormality caused by somatic mutations can result in the production of abnormal proteins and cause a variety of human diseases [12]. Here, we studied 3 LQTS families, in whom a G to A change in the last base of exon 7 (c.1032G>A) was identified. This mutation was previously reported to alter the donor splice-site of intron 7, resulting in the production of exon-skipping transcripts, but not to alter the coded alanine (A344A) [7–9], since it involves the characteristic consensus sequence of the splicing donor site, AG/GUAAGU. *G* at this position is reportedly present in 78% of exons of various genes,

Please cite this article as: Tsuji K, et al, Mechanistic basis for the pathogenesis of long QT syndrome associated with a common splicing mutation in KCNQ1 gene, J Mol Cell Cardiol (2007), doi:10.1016/j.yjmcc.2006.12.015

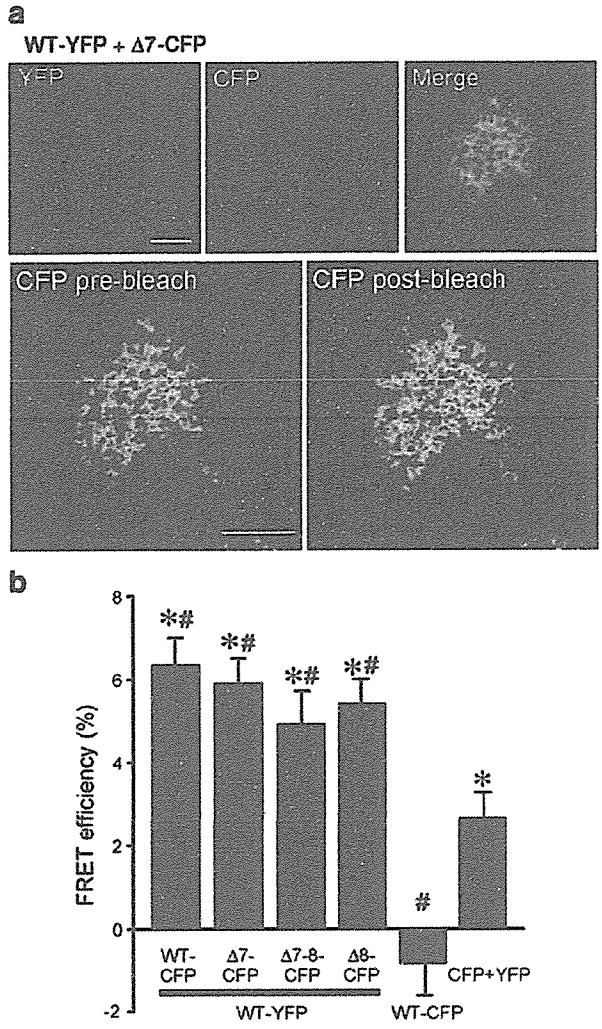

Fig. 6. FRET analysis. (a) WT-YFP and Δ7-CFP were co-expressed in COS7 cells. WT-YFP is pseudocolored in red (left panel) and Δ7-CFP is pseudocolored in green (middle panel). The merged image in the right panel shows co-localization of Δ7-CFP and WT-YFP. Scale bar: 10 μm. (b) Pseudocolor images of Δ7-CFP before (CFP pre-bleach) and after (CFP post-bleach) YFP photobleaching. (c) Summarized data of FRET efficiency. $^{*}p<0.05$ vs. WT-CFP. $^{\#}p<0.05$ vs. CFP+YFP.

and its mutations are responsible for several human diseases, such as Ehlers–Danlos syndrome, Tay–Sachs disease, acute intermittent porphyria, and β-thalassemia [18–21].

Using RT-PCR, we initially confirmed the presence of several short-sized exon-skipping mRNAs (Δ7, Δ7–8, and Δ8) as well as the normal-sized one in peripheral blood lymphocytes from the affected individuals (Fig. 2a). The presence of Δ7–8 and Δ8 mRNAs was previously reported in patients with this mutation [7], but we newly identified a functionally important mutant, Δ7 mRNA, in the present study. We quantitatively showed significant increases of exon-skipping mRNAs (Δ7 and Δ7–8) in the affected individuals compared with normal individuals, who have minor fractions of splicing variants (mostly Δ8), using real-time RT-PCR (Fig. 3c). Interestingly, the mutation at the intron 7 donor splice-site not only affected the binding between exons 7 and 8 but also had significant effects on the binding of exons remote from the mutation: exons 8 and 9, and exons 6 and 9. This observation is noteworthy, considering the fact that splicing mutations are rarely associated with multiple exon skipping [22,23]. Wijk et al. [24] reported a similar case demonstrating the presence of Δ5 and Δ5–6 caused by an intron 5 donor splice-site mutation in the PKLR gene in a patient with pyruvate kinase deficiency. The splice-site recognition of exons may therefore depend on the neighboring exons or introns: the presence of exonic (or intronic) splicing enhancers or silencers in the vicinity of the donor splice-site and acceptor splice-site motifs [25,26] may be involved in our aberrant KCNQ1 splicing, but further studies are needed to prove this hypothesis.

4.2. Functional characterization of exon-skipping KCNQ1 proteins

In the following set of experiments, we aimed to determine the functional characteristics of exon-skipping mutant proteins and to examine their interaction with WT proteins, using electrophysiological and cellular imaging techniques. Current recordings in *Xenopus* oocytes heterologously expressing channels composed of WT or splicing mutant (Δ7, Δ7–8 and Δ8) proteins showed that none of the mutant channels produced measurable currents, and moreover all the mutant proteins displayed the mutant-specific level of dominant-negative effects on WT currents, when co-expressed with WT (Figs. 4a, b).

Confocal microscopy analyses showed that the mutant proteins were retained in an intracellular compartment (presumably, endoplasmic reticulum) and were unable to translocate to the plasma membrane (Fig. 5). Moreover, when WT was co-expressed with mutant proteins, the majority of WT co-localized with the mutants and remained in the intracellular compartment, indicating that the mutants may interfere with the normal trafficking of WT proteins (Fig. 6a). Using FRET analysis, we showed that this occurs because of direct protein–protein interaction between mutant and WT subunits (Fig. 6b). Therefore, the mutants may exert their dominant-negative effect by trapping WT intracellularly and preventing it from translocating to the plasma membrane. A recent report demonstrated that several KCNQ1 mutations cause trafficking errors and the mutant proteins are unable to translocate to the plasma membrane, and some mutations act in a dominant-negative fashion and have the ability to suppress the trafficking of the WT subunit [27,28].

4.3. Genotype-phenotype relationship

cRNAs were introduced in *Xenopus* oocytes in amounts mimicking the proportions of various transcripts of KCNQ1 observed in affected individuals. Ratios simulating those in affected individuals resulted in a pronounced reduction in the whole-cell potassium current, compared with ratios simulating those in normal individuals (Figs. 4c, d). This observation implies that a similar reduction might occur in the potassium current in cardiac myocytes of the mutant carriers, which may

Please cite this article as: Tsuji K, et al, Mechanistic basis for the pathogenesis of long QT syndrome associated with a common splicing mutation in KCNQ1 gene. J Mol Cell Cardiol (2007), doi:10.1016/j.yjmcc.2006.12.015

contribute to the pathogenesis of LQTS. However, it should be noted that the quantitation of mRNA was performed in leukocytes, and it may not accurately reflect the mRNA ratio in the heart. Recently, we reported the identification of a Kcnq1 mutant rat, which carried an intragenic deletion in exon 7 of the Kcnq1 gene [29]. This mutant rat showed deafness due to the marked reduction of endolymph and prolonged QT interval in the ECG, further supporting our hypothesis that the deletion of exon 7 could lead to the phenotypes of LQTS. As far as we could determine, the proportions of mutant mRNAs were comparable in all the affected individuals, despite the fact that the QT_c interval and disease phenotype varied considerably (K-176 II-6: QTc 525 ms, history of syncope, WT: 53.5%, Δ7: 23.4%, Δ7 8: 17.7%, Δ8: 5.4%. K-176 III-2: QTc 404 ms, asymptomatic, WT: 56.6%, Δ7: 20.6%, Δ7–8: 17.7%, Δ8: 5.1%. K-176 III-3: QTc 448 ms, history of syncope, WT: 55.4%, Δ7: 26.5%, Δ7–8: 15.0%, Δ8: 15.0%). This suggests the presence of other modifying factors, which may be genetic or acquired, but the details are unknown.

4.4. Conclusions

We obtained data suggesting the mechanistic basis of the pathogenesis of LQTS caused by a common splicing mutation in KCNQ1. The functional abnormalities of mutant channels observed here may have critical impact on the cellular excitability, and thus contribute to the pathogenesis of LQTS.

Acknowledgments

We thank Dr. Naoyuki Kataoka (Institute for Viral Research, Kyoto University) for his helpful comments and critical reading of the manuscript.

This work was supported by a research grant from the Ministry of Education, Culture, Science, and Technology of Japan (M.H.) and a health sciences research grant (H18-Research on Human Genome-002) from the Ministry of Health, Labour and Welfare of Japan (M.H. and M.A.).

Appendix A. Supplementary data

Supplementary data associated with this article can be found, in the online version, at doi:10.1016/j.yjmcc.2006.12.015.

References

[1] Romano C. Congenital cardiac arrhythmia. Lancet 1965;17:658–9.
[2] Ward OC. A new familial cardiac syndrome in children. J Ir Med Assoc 1964;54:103–6.
[3] Moss AJ, Kass RS. Long QT syndrome: from channels to cardiac arrhythmias. J Clin Invest 2005;115:2018–24.
[4] Barhanin J, Lesage F, Guillemare E, Fink M, Lazdunski M, Romey G. K(V)LQT1 and IsK (minK) proteins associate to form the I(Ks) cardiac potassium current. Nature 1996;384:78–80.
[5] Sanguinetti MC, Curran ME, Zou A, Shen J, Spector PS, Atkinson DL, et al. Coassembly of K(V)LQT1 and minK (IsK) proteins to form cardiac I(Ks) potassium channel. Nature 1996;384:80–3.
[6] Wang Q, Curran ME, Splawski I, Burn TC, Millholland JM, Van Raay TJ, et al. Positional cloning of a novel potassium channel gene: KVLQT1 mutations cause cardiac arrhythmias. Nat Genet 1996;12:17–23.
[7] Murray A, Donger C, Fenske C, Spillman L, Richard P, Dong YB, et al. Splicing mutations in KCNQ1: a mutation hot spot at codon 344 that produces in frame transcripts. Circulation 1999;100:1077–84.
[8] Li H, Chen Q, Moss AJ, Robinson J, Gerstia V, Perry JC, et al. New mutations in the KVLQT1 potassium channel that cause long-QT syndrome. Circulation 1998;97:1264–9.
[9] Kanters JK, Larsen LA, Orholm M, Agner E, Andersen PS, Vuust J, et al. Novel donor splice site mutation in the KVLQT1 gene is associated with long QT syndrome. J Cardiovasc Electrophysiol 1998;9:620–4.
[10] Kramer A. The structure and function of proteins involved in mammalian pre-mRNA splicing. Annu Rev Biochem 1996;65:367–409.
[11] Dreyfuss G, Kim VN, Kataoka N. Messenger-RNA-binding proteins and the messages they carry. Nat Rev, Mol Cell Biol 2002;3:195–205.
[12] Faustino NA, Cooper TA. Pre-mRNA splicing and human disease. Genes Dev 2003;17:419–37.
[13] Jongbloed R, Marcelis C, Velter C, Doeven dans P, Geraedts J, Smeets H. DHPLC analysis of potassium ion channel genes in congenital long QT syndrome. Hum Mutat 2002;20:382–91.
[14] Ishii TM, Silvia C, Hirschberg B, Bond CT, Adelman JP, Maylie J. A human intermediate conductance calcium-activated potassium channel. Proc Natl Acad Sci U S A 1997;94:11651–6.
[15] Zaccolo M. Use of chimeric fluorescent proteins and fluorescence resonance energy transfer to monitor cellular responses. Circ Res 2004;94:866–73.
[16] Gu Y, Di WL, Kelsell DP, Zicha D. Quantitative fluorescence resonance energy transfer (FRET) measurement with acceptor photobleaching and spectral unmixing. J Microsc 2004;215:162–73.
[17] Hastings ML, Krainer AR. Pre-mRNA splicing in the new millennium. Curr Opin Cell Biol 2001;13:302–9.
[18] Weil D, D'Alessio M, Ramirez F, Eyre DR. Structural and functional characterization of a splicing mutation in the pro-alpha 2(I) collagen gene of an Ehlers–Danlos type VII patient. J Biol Chem 1990;265:16007–11.
[19] Akli S, Chelly J, Mezard C, Gandy S, Kahn A, Poenaru L. A "G" to "A" mutation at position −1 of a 5′ splice site in a late infantile form of Tay-Sachs disease. J Biol Chem 1990;265:7324–30.
[20] Grandchamp B, Picat C, de Rooij F, Beaumont C, Wilson P, Deybach JC, et al. A point mutation G→A in exon 12 of the porphobilinogen deaminase gene results in exon skipping and is responsible for acute intermittent porphyria. Nucleic Acids Res 1989;17:6637–49.
[21] Vidaud M, Gattoni R, Stevenin J, Vidaud D, Amselem S, Chibani J, et al. A 5′ splice-region G→C mutation in exon 1 of the human beta-globin gene inhibits pre-mRNA splicing: a mechanism for beta+-thalassemia. Proc Natl Acad Sci U S A 1989;86:1041–5.
[22] Krawczak M, Reiss J, Cooper DN. The mutational spectrum of single base-pair substitutions in mRNA splice junctions of human genes: causes and consequences. Hum Genet 1992;90:41–54.
[23] Nakai K, Sakamoto H. Construction of a novel database containing aberrant splicing mutations of mammalian genes. Gene 1994;141:171–7.
[24] Wijk R, van Wesel AC, Thomas AA, Rijksen G, van Solinge WW. Ex vivo analysis of aberrant splicing induced by two donor site mutations in PKLR of a patient with severe pyruvate kinase deficiency. Br J Haematol 2004;125:253–63.
[25] Fairbrother WG, Yeh RF, Sharp PA, Burge CB. Predictive identification of exonic splicing enhancers in human genes. Science 2002;297:1007–13.
[26] Wang Z, Rolish ME, Yeo G, Tung V, Mawson M, Burge CB. Systematic identification and analysis of exonic splicing silencers. Cell 2004;119:831–45.
[27] Yamashita F, Horie M, Kubota T, Yoshida H, Yumoto Y, Kobori A, et al. Characterization and subcellular localization of KCNQ1 with a heterozygous mutation in the C terminus. J Mol Cell Cardiol 2001;33:197–207.
[28] Wilson AJ, Quinn KV, Graves FM, Bitner-Glindzicz M, Tinker A. Abnormal KCNQ1 trafficking influences disease pathogenesis in hereditary long QT syndromes (LQT1). Cardiovasc Res 2005;67:476–86.
[29] Gohma H, Kuramoto T, Kuwamura M, Okajima R, Tanimoto N, Yamasaki KI, et al. WTC deafness Kyoto (dfk): a rat model for extensive investigations of Kcnq1 functions. Physiol Genomics 2006;24:198–206.

Please cite this article as: Tsuji K, et al, Mechanistic basis for the pathogenesis of long QT syndrome associated with a common splicing mutation in KCNQ1 gene. J Mol Cell Cardiol (2007), doi:10.1016/j.yjmcc.2006.12.015

tapraid2/hrt-hrthm/hrt-hrthm/hrt00207/hrt2400d07z | manjuk | S=1 | 1/15/07 | Art: 2400

N- and C-terminal *KCNE1* mutations cause distinct phenotypes of long QT syndrome

Seiko Ohno, MD,* Dimitar P. Zankov, MD,† Hidetada Yoshida, MD, PhD,* Keiko Tsuji, MS,† Takeru Makiyama, MD,* Hideki Itoh, MD, PhD,† Masaharu Akao, MD, PhD,* Jules C. Hancox, PhD,‡ Toru Kita, MD, PhD,* Minoru Horie, MD, PhD†

*From the *Department of Cardiovascular Medicine, Kyoto University Graduate School of Medicine, Kyoto, †Department of Cardiovascular and Respiratory Medicine, Shiga University of Medical Science, Shiga, Japan, and ‡Department of Physiology, School of Medical Sciences, University of Bristol, Bristol, United Kingdom.*

BACKGROUND Long QT syndromes (LQTS) are inherited diseases involving mutations to genes encoding a number of cardiac ion channels and a membrane adaptor protein. The MinK protein is a cardiac K-channel accessory subunit encoded by the *KCNE1* gene, mutations of which are associated with the LQT5 form of LQTS.

OBJECTIVE The purpose of this study was to search for the *KCNE1* mutations and clarify the function of those mutations.

METHODS We conducted a genetic screen of *KCNE1* mutations in 151 Japanese LQTS patients using the denaturing high-performance liquid chromatography–WAVE system and direct sequencing. In two LQTS patients, we identified two *KCNE1* missense mutations, located in the MinK N- and C-terminal domains. The functional effects of these mutations were examined by heterologous coexpression with *KCNQ1* and *KCNH2*.

RESULTS One mutation, which was identified in a 67-year-old woman, A8V, was novel. Her electrocardiogram (ECG) revealed marked bradycardia and QT interval prolongation. Another mutation, R98W, was identified in a 19-year-old woman. She experienced syncope followed by palpitation in exercise. At rest, her ECG showed bradycardia with mild QT prolongation, which became more prominent during exercise. In electrophysiological analyses, R98W produced reduced I_{Ks} currents with a positive shift in the half activation voltages. In addition, when the A8V mutation was coexpressed with *KCNH2*, this reduced current magnitude, which is suggestive of a modifier effect by the A8V *KCNE1* mutation on I_{Kr}.

CONCLUSION *KCNE1* mutations may be associated with mild LQTS phenotypes, and *KCNE1* gene screening is of clinical importance for asymptomatic and mild LQTS patients.

KEYWORDS Long QT syndrome; *KCNE1*; Ion channels; Molecular screening; Electrophysiology

Introduction

Long QT syndromes (LQTS) are characterized by a prolonged QT interval in the electrocardiogram (ECG) and a high risk of sudden cardiac death due to a characteristic ventricular tachycardia known as torsades de pointes. The syndromes are hereditary based on gene mutations encoding multiple cardiac ion channels and a membrane adaptor protein.[1] In 1996, positional cloning methods established *KCNQ1* as the chromosome 11–linked LQT1 gene.[2] Subsequently, MinK, a potassium channel regulatory subunit encoded by the *KCNE1* gene,[3,4] was shown to coassemble with *KCNQ1* to produce the slowly activating delayed-rectifier K^+ current, I_{Ks}.[5,6] Because of these relationships, MinK was thought to be another candidate for LQTS. At the end of 1997, two groups first identified clinically significant *KCNE1* mutations in LQTS patients.[7,8] Schulze-Bahr and coworkers[7] reported a *KCNE1* compound heterozygous mutation, which induced the Jervell and Lange-Nielsen syndrome (JLNS). The mutations were T7I and D76N, which were located in the N terminus and C terminus of the MinK protein, respectively. Splawski and coworkers[8] also reported two families of the Romano-Ward syndrome and identified two C-terminal *KCNE1* mutations, S74L and D76N. In functional analyses, D76N caused a decreased I_{Ks} current with a strong dominant-negative effect. On the other hand, S74L also decreased I_{Ks} but displayed no dominant-negative effect. Further investigation confirmed the *KCNE1* gene as the fifth LQTS locus (LQT5).[9]

To date, 16 LQT5-related *KCNE1* mutations have been reported, but this number and the incidence of mutations are very small compared with the principal LQTS mutations (LQT1-3). The functional consequences of *KCNE1* mutations in reducing I_{Ks} vary considerably between mutations. Furthermore, the gene-specific phenotype has not been well investigated in LQT5. Here we report two *KCNE1* mutations identified in two Japanese LQTS patients from unre-

MH was supported by Research Grants from the Japan Ministry of Education, Science, Sports and Culture and by Health Science Research Grants from the Japan Ministry of Health, Labor, and Welfare. **Address reprint requests and correspondence:** Minoru Horie, M.D., Ph.D., Department of Cardiovascular and Respiratory Medicine, Shiga University of Medical Science, Seta Tsukinowa-cho, Otsu, Shiga, Japan 520-2192. E-mail address: horie@belle.shiga-med.ac.jp. (Received August 12, 2006; Accepted November 1, 2006.)

lated families, which are located in the N terminus and C terminus. Although these patients had no mutations in LQTS-related genes other than *KCNE1* and relatively mild LQTS phenotypes, the response of QT intervals to heart rates was quite different: QT prolongation became prominent in bradycardia with the N-terminal mutation (A8V) and in tachycardia with the C-terminal mutation (R98W). These heart rate dependencies were compatible with the symptoms of reducing I_{Kr}–rapidly activating delayed-rectifier K^+ current–and I_{Ks}, respectively. Since MinK is also able to coassemble with the HERG protein (encoded by *KCNH2*) and affect the I_{Kr} current,[10–12] we examined the functional influence of these two mutations on both *KCNQ1*- and *KCNH2*-encoded channels, using a heterologous expression system. In this report, we first displayed novel phenotypes of LQT5 that would be caused by reduced I_{Kr}.

Methods

Subjects

The cohort of patients studied was comprised of 151 consecutive LQTS probands showing prolongation in the QT interval (QTc ≥ 460 ms); they were referred to our laboratory for genetic evaluation from all over Japan. The patients had both familial and acquired LQTS. All subjects gave their written informed consent in accordance with guidelines approved by the appropriate institutional review boards. Each underwent detailed clinical and cardiovascular examinations and was then characterized phenotypically on the basis of the QT interval in lead V_5, corrected for heart rate (QTc) according to Bazett's formula, and the presence of cardiac symptoms. Schwartz's scores[13] of all probands were greater than 3 points.

Genotyping

Genomic DNA was isolated from venous blood by use of the QIAamp DNA blood midikit (Qiagen, Hilden, Germany). Established primer settings were employed to amplify the entire coding regions of the known LQTS genes (*KCNQ1*,[14,15] *KCNH2*,[14] *SCN5A*,[16] *KCNE1*,[14] and *KCNE2*[17]), with the exception of *ANKB*[18] from genomic DNA. The denaturing high-performance liquid chromatography (DHPLC; WAVE system Model 3500, Transgenomic, Omaha, NE) technique was performed as described elsewhere.[19] Polymerase chain reaction (PCR) products were denatured at 95°C for 5 minutes and then analyzed in DHPLC. The PCR fragments presenting abnormal signals in DHPLC analysis were subsequently sequenced by the dideoxynucleotide chain termination method with fluorescent dideoxynucleotides on an ABI 3100 genetic analyzer (PE Applied Biosystems).

Site-directed mutagenesis and expression

Complementary DNAs (cDNAs) for human *KCNQ1* (GenBank AF000571) and *KCNE1* (GenBank M26685) were kindly provided by Dr. J. Barhanin (Institut de Pharmacologie Moléculaire et Cellulaire, CNRS, France). The cDNAs were subcloned into pIRES2-EGFP (for *KCNQ1*) and pIRES-CD8 (for both wild-type [WT] and mutated *KCNE1*) vectors, respectively. The cDNAs for human *KCNH2* (GenBank AF363636) were kindly gifted by Dr. M. Sanguinetti (University of Utah, Salt Lake City, UT). The cDNA was subcloned into the pCEP4/CMV vector. MinK mutations were constructed using a Quick Change II XL Site-Directed Mutagenesis Kit according to the manufacturer's instructions (Stratagene, La Jolla, CA). Nucleotide sequence analysis was performed on each variant construct before the expression study. COS7 cells were transiently transfected using 1 μg of pIRES-CD8/*KCNE1* (WT or mutants) and 1 μg of pIRES2-EGFP/*KCNQ1* per 35 mm dish, using fugene6 according to the manufacturer's instructions (Roche Diagnostics, Basel, Switzerland). CHO cells were cotransfected using 1 μg of pIRES-CD8/*KCNE1* (WT or mutants), 1 μg of pCEP4/CMV/*KCNH2* vector, and 0.5 μg of pEGFP-N1/CMV vector to detect the cells with *KCNH2* expression. COS7 or CHO cells that are successfully transfected with *KCNQ1* or *KCNH2* and *KCNE1* cDNAs were selected by green fluorescence and decoration with anti-CD8 antibody-coated beads (Dynabeads CD8; Dynal Biotech, Oslo, Norway).

Electrophysiological experiments and data analysis

Whole-cell patch-clamp recordings were made with pipettes filled with (in mM) KCl 130, KOH 20, Mg-ATP 5, Na-GTP 0.1, EGTA 5, and HEPES 10 (pH 7.2 with KOH), with a resistance of 2.0 to 4.0 MΩ. The external superfusate contained (in mM) NaCl 140, KCl 5.4, $MgCl_2$ 0.5, $CaCl_2$ 1.8, NaH_2PO_4 0.33, glucose 5.5, and HEPES 5 (pH 7.4 with NaOH). Data were filtered at 2 kHz.

Experiments on *KCNQ1* were performed at 37°C using an Axopatch 200A patch-clamp amplifier (Axon Instruments, Foster City, CA) 48–72 hours after transfection. PClamp software (version 9.0, Axon Instruments) was used to generate voltage pulse protocols and for data acquisition. Currents were elicited by depolarizing pulses from a holding potential of −70 mV to test potentials between −50 and +100 mV (with a 10-mV step increment), followed by repolarization to −30 mV to monitor tail current amplitude. Current densities (pA/pF) were calculated for each cell studied by normalizing peak tail current amplitude to cell capacitance. Activation curves were derived from tail currents at −30 mV after stepping to test potentials ranging from −50 to +100 mV.

Whole-cell patch-clamp recordings with *KCNH2* were performed at 37°C using an EPC-8 patch-clamp amplifier (HEKA, Lambrecht, Germany) 48–72 hours after transfection. Data acquisition was performed using PatchMaster acquisition software (HEKA). Currents were elicited by depolarizing pulses from a holding potential of −80 mV to test potentials between −40 and +50 mV (with a 10-mV step increment), followed by repolarization to −60 mV to monitor tail current amplitude. Current densities (pA/pF) were calculated for each cell studied by normalizing peak tail current amplitude to cell capacitance. Activation curves

were derived from tail currents at −60 mV after stepping to test potentials ranging from −40 to +50 mV.

Current voltage relations were fitted with a Boltzmann's function:

$$I_{K,tail} = 1/\{1 + \exp[(V_{1/2} - V_m)/k]\} \quad (1)$$

where $V_{1/2}$ stands for the potential at which the activation is half maximal, V_m is the test potential, and k is the slope factor.

Time constants describing current time courses were obtained by data with single or double exponential functions shown below (equation 2 for single exponential and equation 3 for double exponential):

$$I(t) = A + B\exp(-t/\tau) \quad (2)$$

$$I(t) = A + B\exp(-t/\tau_{fast}) + C\exp(-t/\tau_{slow}) \quad (3)$$

where $I(t)$ means the current amplitude at time t, A, B, and C are constants, and τ refers to the activation/deactivation time constants obtained.

Numerical data are presented as mean ± standard error of the mean. Student's t-test was used to compare data between different groups for electrophysiological measurements. $P < .05$ was considered statistically significant.

Results

Mutation analysis

In 151 LQTS patients from unrelated families, we found two major elution patterns (Figures 1A(a) and 1A(b).) and two abnormal patterns (Figures 1A(c) and 1A(d)) in DHPLC analyses for *KCNE1*. Subsequent DNA sequencing revealed that the wave patterns shown in Figures 1A(a) and 1A(b) were derived from the normal and D85N polymorphism.[20–23] There were 11 patients with heterozygous D85N polymorphism. The third elution pattern (Figure 1A(c)) turned out to be due to a single nucleotide change (23C > T), causing an amino acid substitution denoted A8V, replacing an alanine at residue 8 with a valine (Figures 1B and 1C). The bottom pattern (Figure 1A(d)) was due to a single nucleotide alternation (292C > T) resulting in an amino acid substitution from an arginine at residue 98, designated R98W (Figures 1B and 1D). Both types of aberrant bands were absent in 110 unrelated healthy individuals of the general population. These mutations are located in the N terminus (A8V) and in the C terminus (R98W), respectively (shown schematically in Figure 1B). The two probands carrying *KCNE1* mutations had homozygous G38 and D85 alleles in *KCNE1* and no other mutations in the LQTS-related genes (see the Methods section). Regarding other LQTS-related genes in our cohort, we found 20 mutations from 27 patients in *KCNQ1*, 33 mutations from 37 patients in *HERG*, and 12 mutations from 12 patients in *SCN5A*.

Phenotypic characterization: Case 1

The A8V mutation was identified in a 67-year-old female who had no family history of syncope and premature sudden death. Arrhythmia was initially detected at age 63 years, and

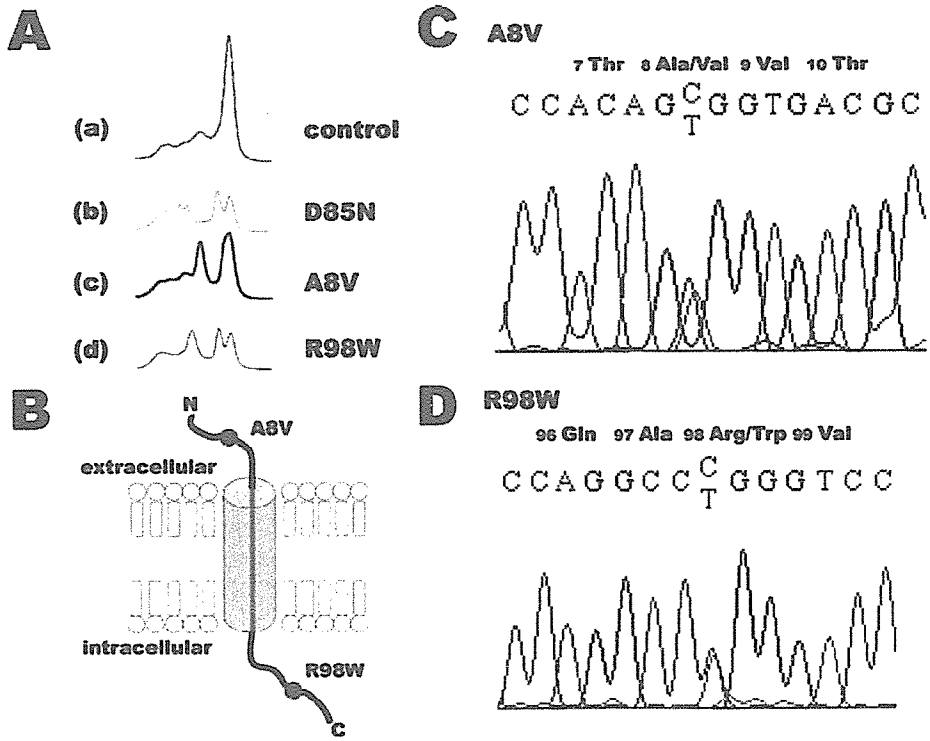

Figure 1 Mutation analysis of *KCNE1*. **A:** DHPLC analyses of PCR products amplifying *KCNE1*: from top to bottom, (a) control, (b) D85N (single nucleotide polymorphism), (c) A8V, and (d) R98W. The control displayed one normal peak pattern; in contrast, D85N, A8V, and R98W displayed two to four peak patterns. **B:** Location of *KCNE1* mutations. **C** and **D:** Sequence analyses for A8V and R98W.

1 month before entering the hospital she began to feel general malaise and palpitations with skipped beats. Her F2 12-lead ECG (Figure 2A(a).) showed prominent sinus bradycardia (46 bpm) and marked QT prolongation (QTc 600 ms) with flat and biphasic T waves in chest leads. After further examination in hospital, paroxysmal atrial fibrillation (AF; Figure 2A(b)) and sinus pause after cessation of AF were detected and were considered to be the cause of her palpitations. Under the diagnosis of bradycardia-tachycardia syndrome, she received a pacemaker implantation. With atrial pacing at 60 bpm, her QTc interval was shortened to within the normal range (QTc 428 ms; Figure 2A(c)).

Phenotypic characterization: Case 2

The R98W mutation was found in a 19-year-old female, an athlete in high school, who experienced several episodes of short-term syncope followed by palpitation during exercise at age 16. In a medical checkup, conducted at the time of entrance to college, sinus bradycardia (heart rate 45 bpm) and mild QT prolongation (QTc 460 ms) were detected on ECG. She was referred for further examination and, during and after a treadmill exercise test (Figures 2B(a) and 2B(b)), her QTc interval prolongation became more prominent. The QTc after 3 minutes of recovery was still prolonged to 580 ms, and a premature ventricular complex was observed (Figure 2B(b)). None of her relatives had a history of syncope or cardiac sudden death.

We were unable to conduct genetic analyses for the relatives of these two index patients because none of them gave informed consent.

Biophysical assays of WT and mutant *KCNE1* channels

To assess the functional consequences of these missense *KCNE1*mutations (A8V and R98W) on the MinK protein, we coexpressed WT and mutant *KCNE1*with either *KCNQ1* F3-4 or *KCNH2* (Figures 3 and 4).

The C-terminal *KCNE1* mutation causes a loss of function of *KCNQ1* channels

Figure 3A shows representative families of current traces recorded from COS7 cells cotransfected with *KCNQ1* and WT or mutant *KCNE1*. Cells expressing WT-*KCNE1*/*KCNQ1* (Figure 3A, left) elicited vigorous outward currents with slow activation/deactivation kinetics, which are typical of I_{Ks} currents as reported elsewhere.[5,6] Cells expressing A8V-*KCNE1*/*KCNQ1* (Figure 3A, middle) revealed different voltage dependence of current activation, although the current amplitude was comparable to that of WT- *KCNE1*. In contrast, R98W-*KCNE1*/*KCNQ1* caused reduced currents compared with WT-*KCNE1* (Figure 3A, right). In the panel of Figure 3, the mean tail current densities measured at −30 mV in multiple measurements were shown plotted as a function of test pulse voltages (between −50 and +100 mV). Mean current densities after the depolarizing test pulse to +20 mV (indicated by arrow) were 12.4 ± 1.8 pA/pF in WT (closed circles), 11.0 ± 1.3 pA/pF in A8V (open circles), and 6.3 ± 1.2 pA/pF in R98W (closed triangles), respectively. Therefore, compared with the WT I_{Ks} channels, R98W (but not A8V) mutant channels carried significantly smaller currents on repolarization from the physiological range of action potential plateau level ($P < .05$ between WT and R98W).

To determine whether or not these mutations altered the voltage dependence of current activation, tail current densities after each test potential were normalized to the maximum value obtained after the test pulse to +100 mV. In Figure 3C, normalized currents were then plotted as a function of test potentials. The curve fits to plotted data points were obtained using equation 1 (see the Methods section). The $V_{1/2}$ and k values derived from these fits were, respectively, +40.0 ± 4.8 and 20.0 ± 1.3 mV for WT, +49.0 ± 4.3 and 23.0 ± 0.8 mV for the A8V mutation, and +55.7 ± 3.8 and 20.4 ± 1.0 mV for R98W mutation. Thus, the A8V produced a positive shift of $V_{1/2}$ by +9 mV (NS vs. WT) and R98V by +16 mV ($P < .05$ vs. WT). Effective outward currents through R98W channels were therefore reduced over a voltage range relevant to the ventricular action potential plateau level.

Time constants for both activation and deactivation were fitted to equation 2 (Methods). In comparison with WT, A8V did not influence the rate of activation, and R98W rather slowed it but there was no statistical significance. τ values at + 40 mV were 1.72 ± 0.31 seconds for WT, 1.55 ± 0.13 seconds for A8V, and 3.20 ± 0.84 seconds for R98W. τ values for deactivation at −30 mV after test pulse to 40 mV were also comparable and were 0.59 ± 0.05 seconds for WT, 0.46 ± 0.03 seconds for A8V, and 0.46 ± 0.04 seconds for R98W.

The N-terminal *KCNE1* mutation causes a loss of function of *KCNH2* channels

Figure 4A shows representative current traces recorded from CHO cells successfully cotransfected with WT or mutant *KCNE1* and *KCNH2*. Cells expressing WT and R98W *KCNE1*/*KCNH2* displayed outward currents with inward rectifying properties (a decline in current during the voltage command at positive test potentials), which are typical of I_{Kr} currents as reported elsewhere (Figure 4A, left and right).[24] In contrast, the magnitude of currents from cells expressing A8V-*KCNE1*/*KCNH2* was reduced (Figure 4A, middle). In Figure 4B, the tail current densities at −60 mV in multiple cells are plotted as a function of test pulse voltages (between −40 and +50 mV). The mean current densities after depolarizing test pulse to +20mV (indicated by arrow in graph) were 85.0 ± 13.4 pA/pF in WT (closed circles), 47.7 ± 6.9 pA/pF in A8V (open circles; $P < .05$ vs. WT), and 75.8 ± 13.8 pA/pF in R98W (closed triangles, NS vs. WT). Therefore, A8V mutant channels carried significantly smaller currents on repolarization from the physiological range of action potential plateau level.

Tail current densities after each test potential were normalized to the maximum value obtained after depolarization to +50 mV. Normalized currents thus calculated are shown

tapraid2/hrt-hrthm/hrt-hrthm/hrt00207/hrt2400d07z | manjuk | S=1 | 1/15/07 | Art: 2400

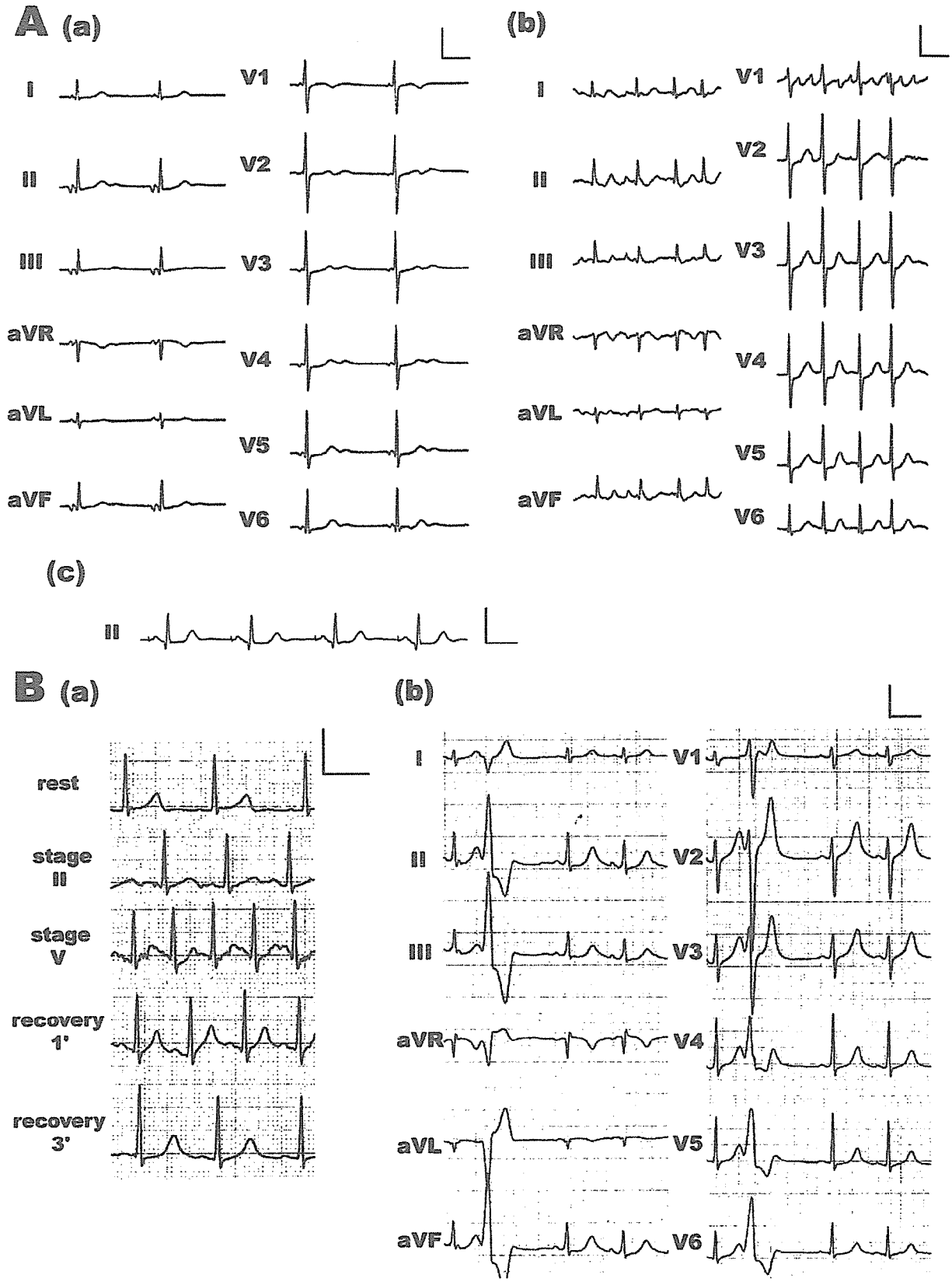

Figure 2 **A:** ECG of case 1: (a) 12-lead ECG at rest, (b) ECG showing AF, (c) lead II strip during atrial pacing at 60 bpm. **B:** ECGs in the case 2: (a) lead V5 strips in treadmill exercise test. With increasing exercise levels, the QT prolongation became more prominent. (b) Twelve-lead ECG at 3 minutes of recovery. Scale bars indicate 1 mV and 400 ms.

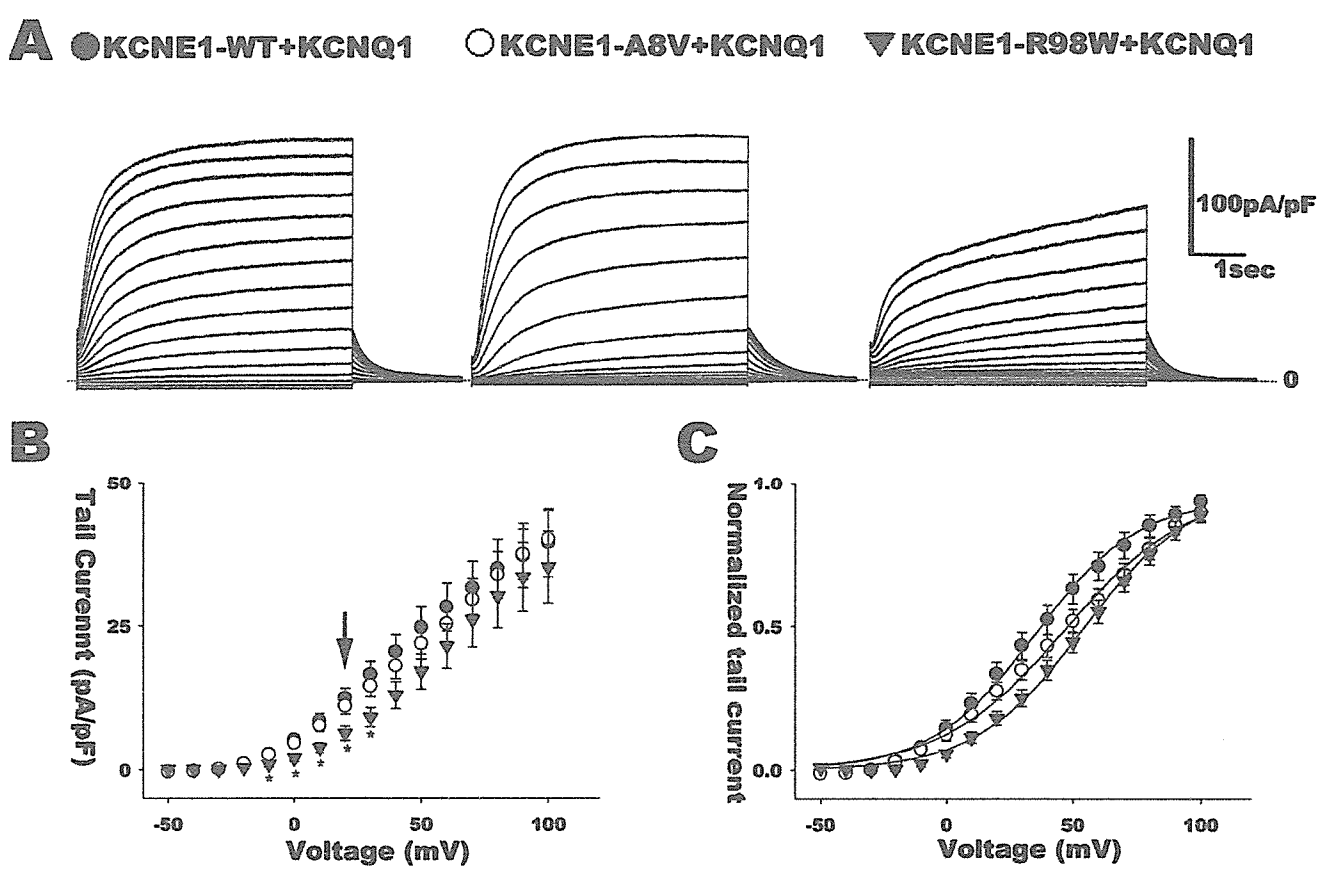

Figure 3 **A:** Current traces recorded from cells expressing *KCNE1*-WT, A8V, or R98W with *KCNQ1*. Currents were elicited from a holding potential of −70 mV, by depolarizing pulses from −50 to +100 mV (with a10-mV step increment) and subsequent repolarization to −30 mV. **B:** Tail current voltage relations for *KCNE1*-WT/*KCNQ1* (*closed circles*, n = 16), A8V/*KCNQ1* (*open circles*, n = 17), and R98W/*KCNQ1* (*closed triangles*, n = 16). $^*P < .05$ versus WT and R98W. **C:** Normalized activation curves.

as a function of test potentials in Figure 4C, and each data set was fitted by equation 1. $V_{1/2}$ and k values were −19.5 ± 0.8 and 7.7 ± 0.4 mV for WT, −25.9 ± 0.8 and 7.9 ± 0.5 mV for A8V, and −19.8 ± 2.3 and 6.9 ± 0.4 mV for R98W, respectively. Therefore, A8V produced a negative shift of $V_{1/2}$ by 6 mV ($P < .05$ vs. WT). Time constants of deactivation were calculated by fitting to equation 3. τ_{fast} and τ_{slow} for tail currents at −60 mV after the +50 mV test pulse were 0.19 ± 0.04 and 1.16 ± 0.21 seconds for WT, 0.25 ± 0.03 and 1.61 ± 0.18 seconds for A8V, and 0.24 ± 0.02 and 1.58 ± 0.09 seconds for R98W, respectively. The values of these time constants did not differ significantly between cells expressing WT and mutant MinK.

Discussion

Clinical features of type 5 LQTS

In the present study, we identified two *KCNE1* mutations in two of 151 unrelated Japanese LQTS probands (1.3%). One of them, A8V, was novel and was identified in an elderly LQTS woman who had paroxysmal AF and sick sinus syndrome. Although her resting ECG displayed marked bradycardia and QT prolongation, her QT interval was normalized after atrial pacing therapy. Recently, *KCNE1* polymorphism (38G) has been shown to be associated with AF.[25] We also found the homozygous 38G allele in the patient, which may be related to her AF. Another mutation, R98W, was found in a young woman athlete who suffered from recurrent short-term syncope only during exercise. Although her ECG displayed only mild QTc prolongation (460 ms), subsequent exercise stress test revealed that her QTc lengthened markedly along with the heart rate increase. We therefore could not rule out the possibility that her symptoms were due to torsades de pointes. Although the R98W mutation has already been reported in an LQTS patient,[26] we could not compare the clinical features of the two cases because no clinical information is available from the previous study.[26]

We were unable to conduct extensive genetic assays for family members of these index patients, but based on their clinical data, both of our patients exhibited a mild LQTS. Biophysical assessment of the *KCNE1* mutants revealed that the newly identified A8V mutation affected significantly the magnitude of expressed *KCNH2* current, leading to a loss-of-function type modulation. Consistent with the functional measurements, our patient with heterozygous A8V mutations showed a definite bradycardia-dependent QT prolongation and sinus bradycardia. The I_{Kr} deactivation process has been implicated as an important part of the pacemaker

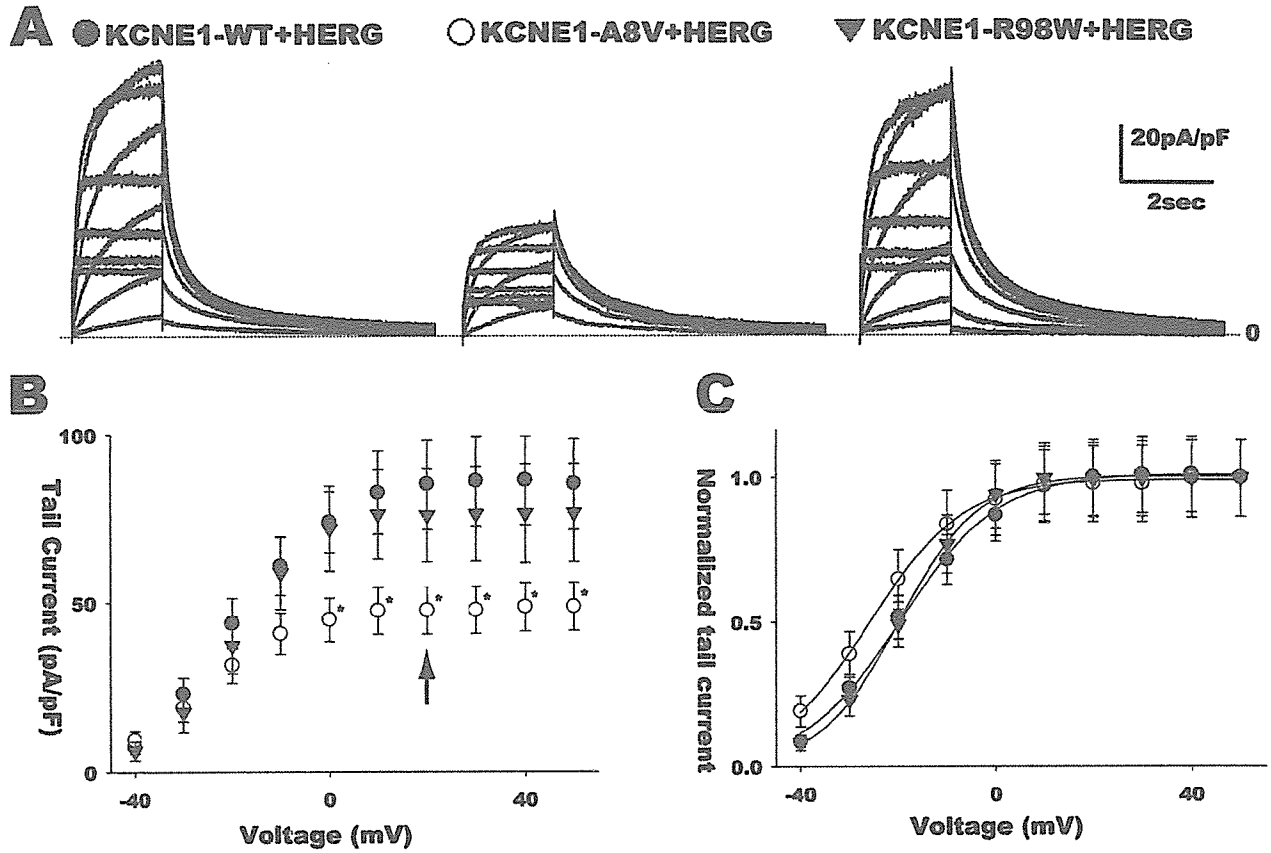

Figure 4 **A:** Current traces recorded from cells expressing *KCNE1*-WT, A8V, or R98W with *KCNH2*. They were elicited from a holding potential of −80 mV by application of depolarizing pulses from −40 to +50 mV (with a 10-mV step increment) and subsequent repolarization to −60 mV. **B:** Tail current voltage relations for *KCNE1*-WT/*KCNH2* (*closed circles*, n = 6), A8V/*KCNH2* (*open circles*, n = 9), and R98W/*KCNH2* (*closed triangles*, n = 8). $P < .05$ versus WT and A8V. **C:** Normalized activation curves.

mechanism,[27] and reduced I_{Kr} may lead to the sinus bradycardia. She had apparently no episodes of torsades de pointes, and her QT interval was normalized after pacing therapy. These features are indeed concordant with a type 2 rather than type 1 LQTS. In addition, our clinical observations suggest that *KCNE1* mutation may be associated with AF in this patient.

MinK encoded by *KCNE1* has been shown to form a stable complex with HERG protein in heterologous coexpression,[11] while MinK-antisense treatment has also been reported to affect I_{Kr} magnitude.[10] Considered together with our observations, this suggests that the A8V MinK mutation may cause a relatively mild LQTS phenotype as a consequence of an altered functional effect on the HERG channel protein. A previously reported *KCNE1* mutation (D76N) has been shown to influence the interaction of MinK with both the KCNQ1 and HERG proteins.[28] However, detailed information on the resulting phenotypes is not available, especially on the rate dependency of QT interval prolongation. To our knowledge, therefore, our A8V case is the first reported example of LQTS exhibiting the phenotype different from type 1 LQTS as a consequence of a *KCNE1* mutation.

Functional analyses of *KCNE1* mutations in N- and C-terminal regions

Until now, only 16 *KCNE1* mutations have been reported, and four of these were homozygous JLNS patients as listed in Table 1. Similar to our cases, Schulze-Bahr and colleagues[29] demonstrated that heterozygous *KCNE1* mutations displayed a relatively mild or even normal phenotype with very low penetrance. This may partially explain why *KCNE1* mutations are more frequently found among JLNS patients. It becomes clinically significant when *KCNE1* mutations produce a severe functional disturbance in a homozygous manner, thereby leading to the JLNS phenotype.

Among 16 *KCNE1* mutations, functional analyses are available on eight mutations (Table 1), four of which were located in the transmembrane segment and the rest in the C terminus. Tapper and George[30] reported that transmembrane and C terminal regions of *KCNE1* interact with the *KCNQ1* protein. Three *KCNE1* mutations in the N terminus have already been reported (T7I,[7] R32H,[26] and R36H[31]), but their functional outcome has not been examined. Alanine at codon 8 is next to threonine at 7[7] and caused a significant modulation on the MinK/HERG complex (Figure 4). Our data therefore raise the possibility that other

Table 1 Summary of all *KCNE1* mutations

Amino acid change	Protein domain	Phenotype	Reference
T7I	N terminal	JLNS*	7
A8V	N terminal	RWS	This study
R32H	N terminal	RWS	26
R36H	N terminal	RWS	31
V47H	Transmembrane	JLNS†	28
L51H	Transmembrane	JLNS†	28
G52R	Transmembrane	RWS	34
F53S	Transmembrane	RWS	31
T59P-L60P	Transmembrane	JLNS	35
K70N	Transmembrane	RWS	36
S74L	C terminal	RWS	8
D76N	C terminal	RWS/JLNS*	7
Y81C	C terminal	RWS	36
W87R	C terminal	RWS	28
R98W	C terminal	RWS	This study, 26
V109I	C terminal	RWS	29
P127T	C terminal	RWS	26

*T7I, D76N; compound heterozygous mutation.
†V47H, L51H; compound heterozygous mutation.

N-terminal mutations may also be of functional importance in the interaction with the HERG protein.

C-terminal *KCNE1* mutations caused various functional changes according to their location and the species of mutated amino acids: the D76N mutation displayed a dominant-negative effect, but S74L caused only current decrease.[8] In general, most C-terminal mutations produced a very mild functional change, and the dominant negative suppression was only seen in D76N. In our experiments, R98W caused a decrease in current density and a positive shift of the activation curve. Melman and colleagues[32] constructed chimeras of *KCNE1* and *KCNE3* and determined the region of *KCNE1* that is necessary and sufficient to modulate the *KCNQ1*. This appeared to be located in the transmembrane portion, which indicates that N- and C-terminal mutations caused no extreme change in I_{Ks} current. This may be one reason why most of the patients with LQT5 mutations in the C terminus showed the rather mild phenotype.

Study limitations

Considering the fact that we did not find any other discernible mutations in the known LQTS genes for the index patients, we employed DHPLC analysis to screen for genetic variants, which may not be 100% effective in the detection of mutations.[33] In DHPLC analysis, although the temperatures of the analysis are optimal, we may miss mutations in the very high or low melting domains. It also cannot be excluded that there might be mutations within regulatory regions or intronic sequences that are important for splicing or transcription.

Conclusion

We have identified two heterozygous mutations that manifested the mild phenotype of LQTS (1.3% incidences among LQTS probands). In the presence of additional risks such as hypokalemia and drugs associated with QT prolongation, however, the arrhythmia risk for these carriers could increase considerably. Therefore, the identification of *KCNE1* mutations with possible phenotypic effects in LQTS patients may be of significant value in providing information important for our understanding of LQT genotype-phenotype correlations. Moreover, in considering the basis for the functional consequences of such mutations, changes to HERG/I_{Kr} as well as KCNQ1/I_{Ks} need to be considered.

Acknowledgments

The authors are grateful to the Japanese LQT families for their willingness to participate in this study. We thank Dr. Andrew F. James, Bristol University, for reading the manuscript.

References

1. Moss AJ, Kass RS. Long QT syndrome: from channels to cardiac arrhythmias. JCI 2005;115:2018–2024.
2. Wang Q, Curran ME, Splawski I, Burn TC, Millholland JM, VanRaay TJ, Shen J, Timothy KW, Vincent GM, de Jager T, Schwartz PJ, Towbin JA, Moss AJ, Atkinson DL, Landes GM, Connors TD, Keating MT. Positional cloning of a novel potassium channel gene: KvLQT1 mutations cause cardiac arrhythmias. Nat Genet 1996;12:17–23.
3. Takumi T, Ohkubo H, Nakanishi S. Cloning of a membrane protein that induces a slow voltage gated potassium current. Science 1988;242:1042–1045.
4. Murai T, Kakizuka A, Takumi T, Ohkubo H, Nakanishi S. Molecular cloning and sequence analysis of human genomic DNA encoding a novel membrane protein which exhibits a slowly activating potassium channel activity. Biochem Biophys Res Commun 1989;161:176–181.
5. Barhanin J, Lesage F, Guillemare E, Fink M, Lazdunski M, Romey G. K_sLQT1 and IsK (minK) proteins associate to form the I_{Ks} cardiac potassium current. Nature 1996;384:78–80.
6. Sanguinetti MC, Curran ME, Zou A, Shen J, Spector PS, Atkinson DL, Keating MT. Coassembly of KvLQT1 and minK (IsK) proteins to form cardiac I_{Ks} potassium channel. Nature 1996;384:80–3.
7. Schulze Bahr E, Wang Q, Wedekind H, Haverkamp W, Chen Q, Sun Y, Rubie C, Hordt M, Towbin JA, Borggrefe M, Assmann G, Qu X, Somberg JC, Breithardt G, Oberti C, Funke H. *KCNE1* mutations cause Jervell and Lange-Nielsen syndrome. Nat Genet 1997;17:267–268.
8. Splawski I, Tristani-Firouzi M, Lehmann MH, Sanguinetti MC, Keating MT. Mutations in the hminK gene cause long QT syndrome and suppress I_{Ks} function. Nat Genet 1997;17:338–340.
9. Duggal P, Vesely MR, Wattanasirichaigoon D, Villafane J, Kaushik V, Beggs AH. Mutation of the gene for IsK associated with both Jervell and Lange Nielsen and Romano Ward forms of long QT syndrome. Circulation 1998;97:142–146.
10. Yang T, Kupershmidt S, Roden DM. Anti-minK antisense decreases the amplitude of the rapidly activating cardiac delayed rectifier K^+ current. Circ Res 1995;77:1246–1253.
11. McDonald TV, Yu Z, Ming Z, Palma E, Meyers MB, Wang KW, Goldstein SA, Fishman GI. A minK HERG complex regulates the cardiac potassium current I_{Kr}. Nature 1997;388:289–292.
12. Tamargo J, Caballero R, Gomez R, Valenzuela C, Delpon E. Pharmacology of cardiac potassium channels. Cardiovasc Res 2004;62:9–33.
13. Schwartz PJ, Moss AJ, Vincent GM, Crampton RS. Diagnostic criteria for the long QT syndrome. An update. Circulation 1993;88:782–784.
14. Splawski I, Shen J, Timothy KW, Vincent GM, Lehmann MH, Keating MT. Genomic structure of three long QT syndrome genes: *KVLQT1*, *HERG*, and *KCNE1*. Genomics 1998;51:86–97.
15. Neyroud N, Richard P, Vignier N, Donger C, Denjoy I, Demay L, Shkolnikova M, Pesce R, Chevalier P, Hainque B, Coumel P, Schwartz K, Guicheney P. Genomic organization of the KCNQ1 K^+ channel gene and identification of C terminal mutations in the long QT syndrome. Circ Res 1999;84:290–297.
16. Wang Q, Li Z, Shen J, Keating MT. Genomic organization of the human SCN5A gene encoding the cardiac sodium channel. Genomics 1996;34:9–16.

AQ: 4

17. Abbott GW, Sesti F, Splawski I, Buck ME, Lehmann MH, Timothy KW, Keating MT, Goldstein SA. MiRP1 forms I_{Kr} potassium channels with HERG and is associated with cardiac arrhythmia. Cell 1999;97:175–187.
18. Mohler PJ, Schott JJ, Gramolini AO, Dilly KW, Guatimosim S, duBell WH, Song LS, Haurogne K, Kyndt F, Ali ME, Rogers TB, Lederer WJ, Escande D, Le Marec H, Bennett V. Ankyrin-B mutation causes type 4 long QT cardiac arrhythmia and sudden cardiac death. Nature 2003;421:634–639.
19. Jongbloed R, Marcelis C, Velter C, Doevendans P, Geraedts J, Smeets H. DHPLC analysis of potassium ion channel genes in congenital long QT syndrome. Hum Mutat 2002;20:382–391.
20. Tesson F, Donger C, Denjoy I, Berthet M, Bennaceur M, Petit C, Coumel P, Schwarts K, Guicheney P. Exclusion of KCNE1 (IsK) as a candidate gene for Jervell and Lange-Nielsen syndrome. J Mol Cell Cardiol 1996;28:2051–2055.
21. Westenskow P, Splawski I, Timothy KW, Keating MT, Sanguinetti MC. Compound mutations: a common cause of severe long QT syndrome. Circulation 2004;109:1834–1841.
22. Paulussen AD, Gilissen RA, Armstrong M, Doevendans PA, Verhasselt P, Smeets HJ, Schulze Bahr E, Haverkamp W, Breithardt G, Cohen N, Aerssens J. Genetic variations of *KCNQ1*, *KCNH2*, *SCN5A*, *KCNE1*, and *KCNE2* in drug induced long QT syndrome patients. J Mol Med 2004;82:182–188.
23. Denjoy I, Berthet M, Gouas L, Simon F, Lupoglazoff JM. A homozygous mutation in KCNE1 cause long-QT syndrome without deafness. Circulation 2004;110(Suppl 3):501.
24. Sanguinetti MC, Jiang C, Curran ME, Keating MT. A mechanistic link between an inherited and an acquired cardiac arrhythmia: *HERG* encodes the I_{Kr} potassium channel. Cell 1995;81:299–307.
25. Lai LP, Su MJ, Yeh HM, Lin JL, Chiang FT, Hwang JJ, Hsu KL, Tseng CD, Lien WP, Tseng YZ, Huang SK. Association of the human minK gene 38G allele with atrial fibrillation: evidence of possible genetic control on the pathogenesis of atrial fibrillation. Am Heart J 2002;144:485–490.
26. Splawski I, Shen J, Timothy KW, Lehmann MH, Priori S, Robinson JL, Moss AJ, Schwartz PJ, Towbin JA, Vincent GM, Keating MT. Spectrum of mutations in long QT syndrome genes. *KVLQT1*, *HERG*, *SCN5A*, *KCNE1*, and *KCNE2*. Circulation 2000;102:1178–1185.
27. Ono K, Ito H. Role of rapidly activating delayed rectifier K^+ current in sinoatrial node pacemaker activity. Am J Physiol 1995;269:H453–462.
28. Bianchi L, Shen Z, Dennis AT, Priori SG, Napolitano C, Ronchetti E, Bryskin R, Schwartz PJ, Brown AM. Cellular dysfunction of LQT5-minK mutants: abnormalities of I_{Ks}, I_{Kr} and trafficking in long QT syndrome. Hum Mol Genet 1999;8:1499–1507.
29. Schulze-Bahr E, Schwarz M, Hatenschild S, Wedekind H, Funke H, Haverkamp W, Breithardt G, Pongs O, Isbrandt D. A novel long QT 5 gene mutation in the C terminus (V1091I) is associated with a mild phenotype. J Mol Med 2001;79:504–509.
30. Tapper AR, George AL Jr. MinK subdomains that mediate modulation of and association with KvLQT1. J Gen Physiol 2000;116:379–389.
31. Napolitano C, Priori SG, Schwartz PJ, Bloise R, Ronchetti E, Nastoli J, Bottelli G, Cerrone M, Leonardi S. Genetic testing in the long QT syndrome: development and validation of an efficient approach to genotyping in clinical practice. JAMA 2005;294:2975–2980.
32. Melman YF, Domenech A, de la Luna S, McDonald TV. Structural determinants of KvLQT1 control by the KCNE family of proteins. J Biol Chem 2001;276:6439–6444.
33. Xiao W, Oefner PJ. Denaturing high performance liquid chromatography: a review. Hum Mutat 2001;17:439–474.
34. Ma L, Lin C, Teng S, Chai Y, Bahring R, Vardanyan V, Li L, Pongs O, Hui R. Characterization of a novel long QT syndrome mutation G52R-KCNE1 in a Chinese family. Cardiovasc Res 2003;59:612–619.
35. Tyson J, Tranebjaerg L, Bellman S, Wren C, Taylor JF, Bathen J, Aslaksen B, Sorland SJ, Lund O, Malcolm S, Pembrey M, Bhattacharya S, Bitner-Glindzicz M. IsK and KvLQT1: mutation in either of the two subunits of the slow component of the delayed rectifier potassium channel can cause Jervell and Lange-Nielsen syndrome. Hum Mol Genet 1997;6:2179–2185.
36. Lai LP, Su YN, Hsieh FJ, Chiang FT, Juang JM, Liu YB, Ho YL, Chen WJ, Yeh SJ, Wang CC, Ko YL, Wu TJ, Ueng KC, Lei MH, Tsao HM, Chen SA, Lin TK, Wu MH, Lo HM, Huang SK, Lin JL. Denaturing high-performance liquid chromatography screening of the long QT syndrome related cardiac sodium and potassium channel genes and identification of novel mutations and single nucleotide polymorphisms. J Hum Genet 2005;50:490–496.

A −786T>C polymorphism in the endothelial nitric oxide synthase gene reduces serum nitrite/nitrate levels from the heart due to an intracoronary injection of acetylcholine

Masafumi Nakayama[a], Michihiro Yoshimura[a], Tomohiro Sakamoto[a], Koji Abe[a], Megumi Yamamuro[a], Makoto Shono[a], Satoru Suzuki[a], Tsunenori Nishijima[a], Yoshihiro Miyamoto[b], Yoshihiko Saito[c], Kazuwa Nakao[d], Hirofumi Yasue[e] and Hisao Ogawa[a]

We identified a −786T>C polymorphism in the eNOS gene, and this polymorphism was strongly associated with coronary spasm. The present study aimed to elucidate whether the −786T>C polymorphism or acetylcholine (ACh)-induced coronary spasm affects serum nitrite/nitrate (NOx) levels. The study population comprised three groups: (i) 26 patients without coronary spasm in the left anterior descending coronary artery (LAD) with the T/T genotype (group A); (ii) 20 patients with coronary spasm in the LAD with the T/T genotype (group B); and (iii) 16 patients with coronary spasm in the LAD with the C/T genotype (group C). Paired blood samples were obtained from the coronary sinus (CS) and the aortic tract (Ao) before and after an intracoronary injection of ACh. Serum NOx and plasma lactate levels were measured. The delta NOx level was calculated as the serum concentration of NOx in the CS minus that in the Ao. We compared lactate extraction ratios (LERs) and delta NOx levels between the three groups. The LERs after the provocation test in groups A, B and C were 18.9±2.4%, −0.5±3.9% and −13.5±4.2%, respectively. The LER in group C was significantly lower than in group B. The delta NOx levels after the provocation test in groups A, B and C were 11.5±1.7 μmol/l, 10.4±3.5 μmol/l and −2.1±4.8 μmol/l, respectively. The delta NOx levels in group C were significantly lower ($P<0.05$). Although the NOx level was significantly increased after the provocation test in group A ($P<0.05$), the NOx level was significantly decreased after the provocation test in group C ($P=0.001$). In group B, the provocation test did not significantly change the delta NOx level. In conclusion, the −786T>C polymorphism reduces the NOx level from the heart due to an intracoronary injection of ACh, and thereby predisposes the patients to severe coronary spasm. *Pharmacogenetics and Genomics* 16:339–345 © 2006 Lippincott Williams & Wilkins.

Pharmacogenetics and Genomics 2006, 16:339–345

Keywords: acetylcholene, coronary vasospasm, endothelium-derived nitric oxide, genetic polymorphism

[a]Department of Cardiovascular Medicine, Graduate School of Medical Sciences, Kumamoto University, Kumamoto, [b]Division of Atherosclerosis and Diabetes, National Cardiovascular Center, Osaka, [c]First Department of Internal Medicine, Nara Medical University, Nara, [d]Department of Medicine and Clinical Science, Kyoto University Graduate School of Medicine, Kyoto and [e]Division of Cardiology, Kumamoto Aging Research Institute, Kumamoto, Japan.

Correspondence and requests for reprints to Michihiro Yoshimura, Department of Cardiovascular Medicine, Kumamoto University School of Medicine, 1-1-1 Honjo, Kumamoto 860-8556, Japan.
Tel: +1 81 96 3735175; fax: +1 81 96 3623256;
e-mail: bnp@kumamoto-u.ac.jp

Sponsorship: This study was supported in part by the following grants: Japan Heart Foundation Research Grant 14C-4 for Cardiovascular Disease from the Ministry of Health and Welfare; and Grants-in-Aid for Scientific Research B2-15390248, B2-15390249 and C2-14570680 from the Ministry of Education, Science and Culture, Tokyo, Japan.

Received 21 July 2005 Accepted 28 December 2005

Introduction

Coronary spasm plays an important role in the pathogenesis of not only variant angina, but also of ischemic heart diseases in general, including other forms of angina pectoris, acute myocardial infarction, and sudden death [1]; however, the precise mechanism of the pathogenesis remains to be elucidated.

We have shown that an intracoronary injection of acetylcholine (ACh) results in severe vasoconstriction in coronary spasm patients, whereas ACh causes coronary vasodilation in subjects with healthy coronary arteries [1–3]. ACh-induced vasodilation is mediated by NO released from the endothelium [4,5]. These results suggest that the endothelium in the coronary arteries of coronary spasm patients is dysfunctional and that, as a consequence, NO release in response to ACh is lessened. Indeed, we have previously shown that basal, ACh-stimulated and flow-dependent NO activities are decreased in both the coronary and brachial arteries of coronary spasm patients [6,7].

In the endothelium of both animals and humans, the synthesis of nitric oxide (NO) from the amino acid

1744-6872

L-arginine is catalysed by the endothelial nitric oxide synthase (eNOS) enzyme [4], and the resulting continuously generated NO serves to maintain basal vascular tone [4,5]. We previously reported that the –786T > C polymorphism in the 5′-flanking region of the eNOS gene was an independent risk factor for coronary spasm, as was smoking, although to a lesser degree [8,9]. As assessed by reporter gene assays, the –786C allele resulted in a significant reduction in eNOS gene promoter activity [8]. We also reported that the replication protein A1 represses the eNOS gene with the –786C allele, acting as a repressor of the eNOS gene transcription [10].

The present study aimed to elucidate whether an intracoronary injection of ACh increases NO production from the heart in coronary spasm patients and in non-coronary spasm patients; moreover, whether and how the –786T > C polymorphism of the eNOS gene affects NO levels from the heart.

Materials and methods

Study population

We analysed 64 subjects who were admitted consecutively at Kumamoto University Hospital. All subjects underwent coronary angiography with an intracoronary injection of ACh for evaluation of chest pain. Coronary spasm is defined as total or subtotal occlusion of the coronary artery associated with chest pain and/or ischemic electrocardiographical changes. After an intracoronary injection of isosorbide dinitrate (ISDN), the patients' coronary arteries appeared to be normal and exhibited no significant organic stenosis (< 50% luminal diameter).

Subsequently, we divided these subjects into three groups: (i) 26 T/T genotype patients who had no coronary spasm in the left coronary arteries (group A); (ii) 20 T/T genotype patients who had coronary spasm in the left coronary arteries after an intracoronary injection of ACh (group B); and (iii) 16 C/T genotype patients who had coronary spasm in the left coronary arteries after an intracoronary injection of ACh (group C). There were two C/T genotype patients without coronary spasm in the left coronary arteries. There were no patients with the C/C genotype.

When considering the clinical characteristics of the study patients, hypertension was operationally defined as a blood pressure > 145/90 mmHg, whereas diabetes mellitus was defined as fasting venous blood glucose levels ≥ 126 mg/dl or > 200 mg/dl on an oral glucose tolerance test. Cigarette smoking included current smokers and ex-smokers.

Written informed consent was obtained from all patients. The study was also in agreement with the guidelines of and approved by the ethics committee of Kumamoto University Graduate School of Medical Sciences.

Cardiac catheterization

All medications being taken by the study participants were discontinued at least 48 h prior to cardiac catheterization. Coronary arteriography was performed in the morning when the subjects were in a fasting state. After baseline arteriography of the left and right coronary arteries, an intracoronary injection of ACh was administrated, as previously described [3]. Two consecutive doses (50 and 100 μg) of ACh were injected, 4 min apart, into the left coronary artery; angiography was performed, and completed within 30 s of each injection. Then, 50 μg of ACh was injected into the right coronary artery and angiography was again performed 4 min apart. Finally, both left and right coronary arteriograms were taken after an intracoronary injection of 1 mg of ISDN. We evaluated the degree of organic stenosis after the injection of ISDN.

Blood sampling and assays

Paired blood samples were obtained from the aorta and the coronary sinus immediately following the injection of 100 μg of ACh into the left coronary artery and these samples were then immediately placed in an ice bath. After centrifuging of the blood sample for 10 min, the serum and plasma were packed in a freezer at –80°C for subsequent determination of nitrite/nitrate and lactate concentrations.

Screening for the –786T>C polymorphism of the eNOS gene by the allele-specific oligonucleotide method

The allele-specific oligonucleotide method was used to determine the presence of the –786T > C polymorphism. This method has been described previously [9]. In brief, polymerase chain fragments 236-bp in length, including the –786T/C site, were blotted in duplicate onto nylon membranes. Hybridization was accomplished with ^{32}P-radiolabelled oligonucleotides corresponding to either the –786T sequence (5′-GGG TCA GCC AGC CAG GGA A-3′: probe for the –786T sequence) or the –786C sequence (5′-GGG TCA GCC GGC CAG GGA A-3′: probe for the –786C sequence).

Measurement of plasma lactate concentration and serum nitrite/nitrate concentration

Plasma lactate concentrations were measured using an enzyme assay [12]. We determined the lactate extraction ratio (LER) as: 100 × [plasma lactate concentration at aorta (Ao)–plasma lactate concentration at coronary sinus (CS)]/lactate concentration at Ao. Serum nitrite/nitrate concentrations were measured using a flow injection autoanalyser (TCI-NOX1000, Tokyo Kasei Kogyo, Tokyo, Japan) which is based on the Griess Reaction methodology [11]. The samples were passed through a column containing copper-coated cadmium, which reduced all nitrate to nitrite; the nitrite was then detected by

reacting it with a Griess reagent; and, finally, nitrite/nitrate concentrations were then measured spectrophotometrically at 540 nm.

We analysed delta serum nitrite/nitrate (NOx) levels as: NOx concentration at the CS–NOx concentration at the Ao.

Statistical analysis

Continuous variables were compared using two-tailed unpaired *t*-tests. Categorical variables were compared by chi-square analysis with Fisher's exact probability test. LER and delta NOx levels were compared using two-tailed unpaired *t*-tests between the study groups. Comparison of delta NOx levels before and after an intracoronary injection of ACh was performed using the paired *t*-test. Linear regression analysis was used to correlate delta NOx level and LER. $P < 0.05$ was considered statistically significant.

Results

Clinical characteristics of the study population

The clinical characteristics of this study population are shown in Table 1. There were no significant differences between the three groups regarding age, gender, cigarette smoking, hypertension, diabetes mellitus, total cholesterol level, or body mass index.

Lactate extraction ratios

Before an intracoronary injection of ACh, LERs in groups A, B and C were $39.0 \pm 2.3\%$, $36.1 \pm 2.7\%$ and $36.3 \pm 3.1\%$, respectively (Fig. 1). There were no significant differences between the three groups. After an intracoronary injection of ACh, LERs in groups A, B and C were $19.0 \pm 2\%$, $-0.5 \pm 4\%$ and $-13.5 \pm 4\%$, respectively (Fig. 1). In the patients with the –786T/T genotype, LER was significantly lower in the patients with coronary spasm (group B) than in the patients without coronary spasm (group A) ($P < 0.0001$). In the coronary spasm patients, LER was significantly lower in the patients with the –786C/T genotype (group C) than in the patients with the –786T/T genotype (group B) ($P < 0.03$). The LERs in two patients with the –786C/T genotype, without coronary spasm, were 63.4% and 6.3% after an intracoronary injection of ACh.

Serum nitrite/nitrate levels

Serum NOx levels in the aorta and the coronary sinus before and after the provocation test are shown in Table 2 There were no significant differences in the serum NOx levels between the three groups regarding each part or blood sampling time. Subsequently, we analysed the delta NOx level as: NOx at the CS–NOx concentration at the Ao.

Before the provocation test, the delta NOx levels in groups A, B and C were 7.6 ± 2.2 μmol/l, 12.9 ± 3.8 μmol/l and 14.8 ± 3.9 μmol/l, respectively (Fig. 1). There were no significant differences between the three groups. After the provocation test, the delta NOx levels in groups A, B and C were 11.5 ± 1.7 μmol/l, 10.4 ± 3.5 μmol/l and -2.1 ± 4.8 μmol/l, respectively (Fig. 1). The delta NOx levels in group C were significantly lower ($P < 0.05$). We compared the delta NOx levels before and after the provocation test in each group as shown in Fig. 2. Although the delta NOx level was significantly increased after the provocation test in group A ($P < 0.05$), the delta NOx level was significantly decreased after the provocation test in group C ($P < 0.001$). In group B, the provocation test did not significantly change the delta NOx level. In one of the two patients with the –786C/T genotype without coronary spasm, the delta NOx levels before and after the provocation test were 46.5 μmol/l and 38.1 μmol/l, respectively; the delta NOx levels of the other patient before and after the provocation test were 20.3 μmol/l and 18.4 μmol/l, respectively. The delta NOx levels in the two patients with the –786C/T genotype without coronary spasm basically decreased after the provocation test.

Correlation between delta NOx level and LER

Before the provocation test, the delta NOx level did not significantly correlate with LER ($r = -0.042$, $P = $ NS) (Fig. 3). After the provocation test, the delta NOx level had a significant positive correlation with LER ($r = 0.346$, $P < 0.005$) (Fig. 3).

Discussion

The vascular endothelium plays an important role in the regulation of regional blood flows by releasing an endothelium derived relaxing factor, a major component

Table 1 Clinical characteristics of the study subjects

	Group A: non-coronary spasm with –786T/T (n=26)	Group B: coronary spasm with –786T/T (n=20)	Group C: non-coronary spasm with –786C/T (n=16)	P
Age (years)	61±13	64±9	60±15	NS
Men : women (ratio)	12 : 14	10 : 10	9 : 7	NS
Cigarette smoking, n (%)	10/26 (38)	10/20 (50)	10/16 (63)	NS
Hypertension, n (%)	8/26 (31)	8/20 (40)	4/16 (25)	NS
Diabetes mellitus, n (%)	1/26 (4)	4/20 (20)	4/26 (25)	NS
Total cholesterol (mg/dl)	184±29	187±24	184±35	NS
Body mass index (kg/m^2)	24.0±3.2	23.0±1.5	23.5±3.7	NS

Data are mean±SD except where indicated.

Fig. 1

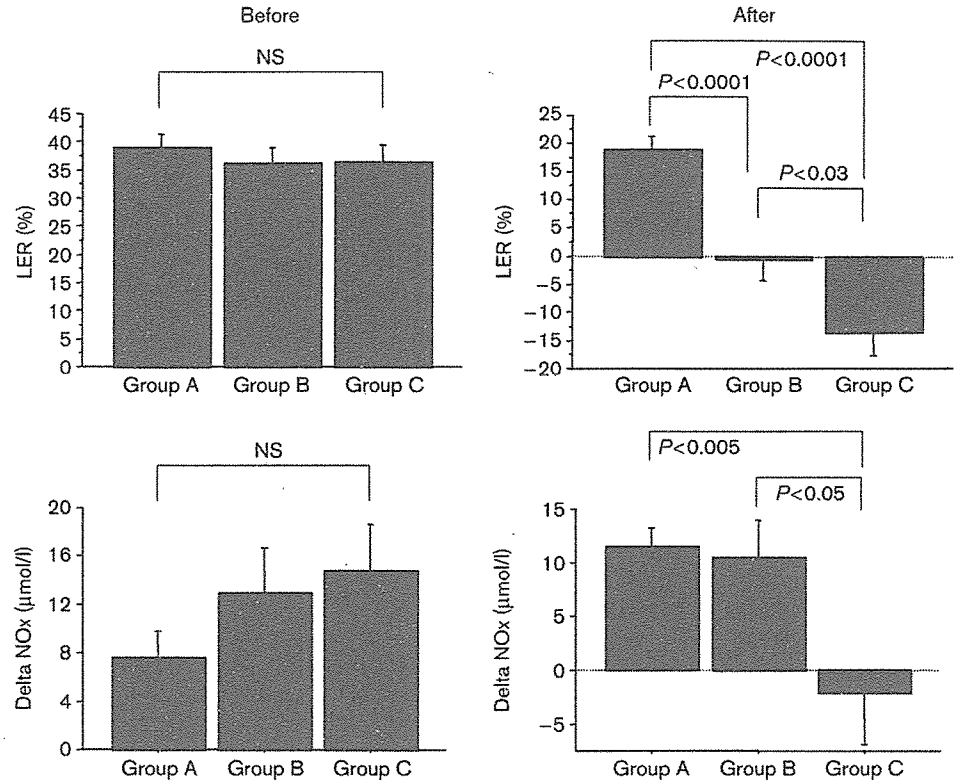

Lactate extraction ratio (LER) before (left) and after (right) an intracoronary injection of acetylcholine. Delta nitrite/nitrate (NOx) levels before (left) and after (right) an intracoronary injection of acetylcholine. The delta NOx indicates the difference in serum NOx level between the coronary sinus (CS) and the aorta (Ao) [delta NOx (CS–Ao)]. Values are expressed as the means ± SEM.

Table 2 **Serum nitrite/nitrate levels (μmol/l) in aorta and coronary sinus before and after provocation test**

	Before		After	
	Aorta	Coronary sinus	Aorta	Coronary sinus
Group A: non-coronary spasm with −786T/T (n=26)	54.9±31.2	62.4±34.1	41.1±27.0	52.7±30.5
Group B: coronary spasm with −786T/T (n=20)	45.1±22.2	58.0±24.8	38.1±18.9	48.4±20.8
Group C: non-coronary spasm with −786C/T (n=16)	49.9±21.8	64.7±22.9	52.1±29.5	50.0±15.8

Data are mean ± SD.

of which is endothelial NO [4,5]. An intracoronary injection of ACh results in severe vasoconstriction in coronary spasm patients, whereas ACh causes coronary vasodilation in subjects with healthy coronary arteries [1–3]. ACh-induced vasodilation is mediated by NO released from the endothelium [4,5]. Because NO is a labile substance with a short half-life and decomposes rapidly into nitrite and nitrate (NOx), its direct measurement has proved to be difficult [13]. It has been reported that increases in the serum NOx levels in rats treated with endotoxin were inhibited by the coadministration of NO synthase inhibitor nitro-L-argine methyl ester, suggesting that the NOx level reflects endogenous NO production [14].

In the present study in coronary spasm patients, LER was significantly lower in the patients with the –786C/T genotype of the eNOS gene than in the patients with the –786T/T genotype after an intracoronary injection of ACh. The –786T > C polymorphism possibly causes coronary spasm and contributes to the severity. Naber *et al.* [15] reported that myocardial lactate uptake was reversed into net lactate production after an intracoronary injection of acetylcholine in subjects with the –786C allele. Our results on LER is in agreement with their report. As for possible actions to increase the severity of coronary spasm, the –786C > T polymorphism significantly reduced delta NOx levels in coronary spasm patients after the provocation test.